scientific reports

Check for updates

OPEN

Bilirubin, a hepatoprotective agent that activates SIRT1, PGC-1α, and PPAR-α, while inhibiting NF-κB in rats with metabolic-associated fatty liver disease

Motahareh Taghizadeh[1,2], Mohammad Hasan Maleki[2], Omid Vakili[3], Ramin Tavakoli[1,2], Parvin Zarei[4], Amirreza Dehghanian[5,6], Hossein Bordbar[7,8] & Sayed Mohammad Shafiee[9]✉

Metabolic-associated fatty liver disease (MAFLD) is a chronic liver disorder characterized by fatty liver disease alongside overweight or obesity and/or type 2 diabetes mellitus (T2DM). Timely intervention is crucial for a potential cure. This study aimed to investigate the effects of bilirubin, an endogenous antioxidant, on lipid metabolism and inflammation in MAFLD. Specifically, it examined bilirubin's impact on SIRT1, PPAR-α, and NF-κB in the livers of rats with MAFLD induced by a high-fat diet (HFD) and streptozotocin (STZ) administration. Forty eight-week adult male Sprague Dawley rats were divided into five groups (n = 8): Control, HFD-STZ, HFD-S-BR6, HFD-S-BR14, and C-BR14. In the last three groups, bilirubin administration was performed intraperitoneally for 6 and 14 weeks (10 mg/kg/day). We selected the key genes associated with MAFLD and subsequently performed GO (Gene Ontology) and KEGG (Kyoto Encyclopedia of Genes and Genomes) analyses to explore the enriched biological processes and signaling pathways. Hence, the gene expression of SIRT1, PGC-1α, PPAR-α, and inflammatory genes (NF-κB, TNF-α, IL-6, and IL-1β) was measured using Real-time quantitative PCR. Stereological and histopathological alterations of liver structure as well as lipid profile, biochemical indices, and liver indices, were also assessed among different groups. The enrichment analysis identified that several signaling pathways and biological processes might be related to MAFLD. Bilirubin-treated rats contained higher PPAR-α, PGC-1α, and SIRT1 expression levels by approximately 5.7-, 2.1-, and 2.2-fold, respectively, compared to the HFD-receiving rats ($p < 0.0001$, $p < 0.05$, and $p < 0.05$). Whereas, the genes involved in the inflammatory cascades, including NF-κB, TNF-α, and IL-6, were downregulated by 0.6-fold ($p < 0.05$) following 14-week treatment of bilirubin, while only significantly decreased expression of NF-κB and IL-6 (approximately 0.6-fold, $p < 0.05$) were observed after 6-week treatment of bilirubin. Remarkably, bilirubin administration favorably reversed the effects of HFD on the liver's volume and cell numbers and ameliorated the related structural changes. It also improved lipid profile, biochemical parameters, and liver indices of HFD-STZ rats. This study indicated that bilirubin acts as a protective/ameliorative compound against MAFLD, particularly through regulating the key genes involved in lipid metabolism and inflammation in HFD-STZ rats.

Keywords Metabolic associated fatty liver disease, Bilirubin, SIRT1, PPAR-α, NF-κB, Inflammation

[1]Student Research Committee, School of Medicine, Shiraz University of Medical Sciences, Shiraz, Iran. [2]Department of Clinical Biochemistry, School of Medicine, Shiraz University of Medical Sciences, Shiraz, Iran. [3]Department of Clinical Biochemistry, School of Pharmacy and Pharmaceutical Sciences, Isfahan University of Medical Sciences, Isfahan, Iran. [4]Department of Bioinformatics, School of Advanced Technologies in Medicine, Isfahan University of Medical Sciences, Isfahan, Iran. [5]Trauma Research Center, Shiraz University of Medical Sciences, Shiraz, Iran. [6]Molecular Pathology and Cytogenetics Division, Department of Pathology, School of Medicine, Shiraz University, Shiraz, Iran. [7]Histomorphometry and Stereology Research Center, Shiraz University of Medical Sciences, Shiraz, Iran. [8]Department of Anatomy, School of Medicine, Shiraz University of Medical Sciences, Shiraz, Iran. [9]Autophagy Research Center, Department of Clinical Biochemistry, School of Medicine, Shiraz University of Medical Sciences, Shiraz, Iran. ✉email: shafieem@sums.ac.ir

Abbreviations

MAFLD	Metabolic associated fatty liver disease
MASH	Metabolic associated steatohepatitis
PPAR-α	Peroxisome proliferator-activated receptor-alpha
RXR	Retinoid X receptor
NF-κB	Nuclear factor kappa B
TNF-α	Tumor necrosis factor-alpha
IL-6	Interleukin 6
IL-1β	Interleukin-1 beta
SIRT1	Silent information regulator sirtuin 1
PGC-1α	PPAR gamma coactivator 1 alpha
HFD	High-fat diet
STZ	Streptozotocin
RT-q PCR	Reverse transcription-quantitative polymerase chain reaction
PPREs	PPAR response elements
ER	Endoplasmic reticulum

Metabolic associated fatty liver disease (MAFLD), a chronic liver disorder defined inclusively as the presence of fatty liver disease concomitantly with the presence of overweight or obesity and/or type 2 Diabetes mellitus (T2DM), is a growing health concern worldwide, and serious action is needed for its management[1]. It has been suggested that the presence of metabolic syndrome indicators, such as obesity, hyperglycemia, dyslipidemia, and inflammation might be key driving forces in MAFLD pathogenesis. In this context, a sedentary lifestyle and being on a high-fat diet can exacerbate the disease conditions[2–4]. Currently, there are no definitive medications approved by the Food and Drug Administration (FDA) against MAFLD, and in most cases, MAFLD and the later MASH are usually asymptomatic until the disease progresses to the end stage, when a liver transplant is the only therapeutic option available. Therefore, early diagnosis and intervention may be useful to identify people who have the potential to develop more advanced stages of such devastating disorder[5,6].

It is conceivable that the management of lipid metabolism is regarded as the first measure to be taken to control MAFLD. In this regard, lipid metabolism in the liver is controlled by a highly dynamic transcriptional regulatory network. These regulatory factors include members of nuclear receptors, particularly PPAR-α, which is highly expressed in the liver[7]. This class of nuclear receptors form heterodimers with retinoid X receptor (RXR) and act as lipid sensors through direct binding to a variety of lipids and their derivatives[8]. Upon lipid binding, the transcription of a family of genes involved in lipid homeostasis is modulated, leading to the control of hepatic and the whole-body energy metabolism in response to nutrient availability. Therefore, PPAR-α is an important metabolic sensor that provides the possibility of adjusting the rate of lipid metabolism, and lipogenesis in response to feeding and starvation[8,9]. In addition to its role in regulating metabolism, PPAR-α also has anti-inflammatory effects through the negative regulation of NF-κB[10]. NF-κB is a key transcription factor that triggers the downstream inflammatory cascade such as TNF-α, IL-6, and IL-1β, which bolsters NF- κB activation by creating a feedback loop[11].

Recent evaluations have indicated that SIRT1 also plays a substantial role in regulating transcriptional networks in different pathophysiological circumstances. Remarkably, SIRT1's function depends on the presence of NAD^+, which is also an indicator of cellular energy status[12,13]. SIRT1 can also directly deacetylate and activate its downstream targets, such as PGC-1α, further leading to the regulation of energy homeostasis and lipid metabolism[14]. Additionally, NF-κB and SIRT1 signaling pathways inversely interact with each other to maintain metabolism and energy in balance with the inflammatory response[15]. Together, it is tempting to speculate that there is an interaction between SIRT1, PGC-1α, and PPAR-α relative to the regulation of lipid metabolism, as well as inflammation, inside the liver[16]. Henceforth, a better understanding of whether the management of MAFLD by PPAR-α ligands or SIRT1 activators leads to liver fat reduction or not can be valuable in designing potential therapeutic approaches.

For an extended period, bilirubin, a byproduct of heme catabolism, was traditionally regarded as an indicator of liver dysfunction[17,18]. However, recent decades have seen a shift in this perspective, with bilirubin being proposed as a potential endogenous antioxidant and anti-inflammatory agent capable of exerting protective effects against various inflammatory conditions, including metabolic syndrome, diabetic nephropathy, atherosclerosis, cancer, and fatty liver diseases[19–23]. Notably, numerous studies have demonstrated the beneficial effects of bilirubin in both animal and cellular models, contributing to the amelioration of fatty liver disease[24,25].

Previous literature indicates that mild unconjugated hyperbilirubinemia is associated with lipid-lowering effects and a reduced risk of developing and progressing non-alcoholic fatty liver disease[26–28]. Initially, these effects were attributed to the robust antioxidant properties of bilirubin[29]; however, emerging evidence suggests that they may also result from bilirubin's role in modulating signaling pathways through protein phosphorylation and activating nuclear receptors such as PPAR-α[30,31]. Consequently, recent research has proposed a novel function for bilirubin as a metabolic hormone and a significant signaling molecule with potential therapeutic implications[32,33].

Considering the unrecognized beneficial effects of bilirubin, it drew our attention as a potent therapeutic agent to improve MAFLD and its related complications. Thereby, the current investigation aimed to study the effect(s) of bilirubin, as a potential therapeutic compound, on the activation of PPAR-α- and SIRT1-dependent pathways and decreasing inflammation with a focus on lipid metabolism in the liver of rat models of MAFLD induced by HFD-STZ administration. Here, we also intended to assess stereological and histopathological alterations of the liver tissue following the bilirubin treatment.

Materials and methods

Animals

We bought 48-week-old male Sprague Dawley rats from the Animal Breeding Center at Shiraz University of Medical Science in Shiraz, Iran. The rats' initial weight ranged from 180 to 220 g. Before the studies began, all the animals were housed in an environment that was carefully controlled (temperature: 25 °C ± 2 °C; relative humidity: 25–35%) and provided with free access to normal food and water for one week in order to acclimate them to the conditions of the laboratory. The Shiraz University of Medical Sciences' Institutional Animal Ethics Committee gave the study ethical approval (IR.SUMS.AEC.1401.066). Additionally, every procedure was carried out in compliance with all applicable rules and laws.

Experimental design

Five groups of animals were randomly assigned as follows: (I) The control group (n = 8) consisted of rats maintained on a normal diet and treated with oleoylethanolamide, which served as a vehicle for modified oleic acid, for a duration of 14 weeks; (II) The high-fat diet (HFD)-streptozotocin (STZ) group (n = 7) also received oleoylethanolamide for 14 weeks; (III) The treated group (n = 8) was administered oleoylethanolamide alone for the first 8 weeks, followed by a combination of oleoylethanolamide and 10 mg/kg/day bilirubin for the subsequent 6 weeks; (IV) The protected group (n = 6) comprised HFD-STZ rats treated with 10 mg/kg/day bilirubin for a total of 14 weeks; (V) The C-BR14 group represented healthy rats (n = 8) that received only 10 mg/kg/day bilirubin for 14 weeks (Fig. 1).

The composition of the HFD was 77% fat and sucrose, 14% protein, and 9% carbohydrates (Table 1)[34]. Five minutes prior to each injection, streptozotocin (STZ) at a dosage of 35 mg/kg (Sigma-Aldrich, USA; Cat. No. S0130) was prepared in a 0.1 M citrate buffer with a pH of 4.5. Throughout the duration of the experiment, STZ was protected from light exposure. Following an 8 week dietary adjustment period, an intraperitoneal injection of the prepared STZ was administered[35]. Based on serum bilirubin levels reported in individuals with Gilbert's syndrome and humanized mice models of the condition with transgenic expression of the human UGT1A1*28 genotype, the injectable dose of bilirubin was chosen. A dose of 10 mg/kg/day (17 µmol/kg/day) was determined to be the appropriate intraperitoneal (I.P.) injection dosage[36]. Following the administration of the specified dose, serum levels of total bilirubin were observed to increase nearly twofold. We also investigated the effects of administering 20 and 30 mg/kg/day of bilirubin to each rat, which resulted in an increase in mortality rates after one week. This constituted a pilot study. Notably, no fatalities were recorded at the dosage of 10 mg/kg/day of bilirubin. Consequently, the appropriate dosage of bilirubin was subsequently determined based on the survival outcomes of the rats during these preliminary investigations[20,37]. Parenthetically, the unconjugated bilirubin powder (Sigma Aldrich, USA; Cat. No. B4126) was dissolved in oleoylethanolamide (Sigma–Aldrich, USA; Cat. No. O0383), as the modified oleic acid. The duration required to establish the HFD-STZ model provided a

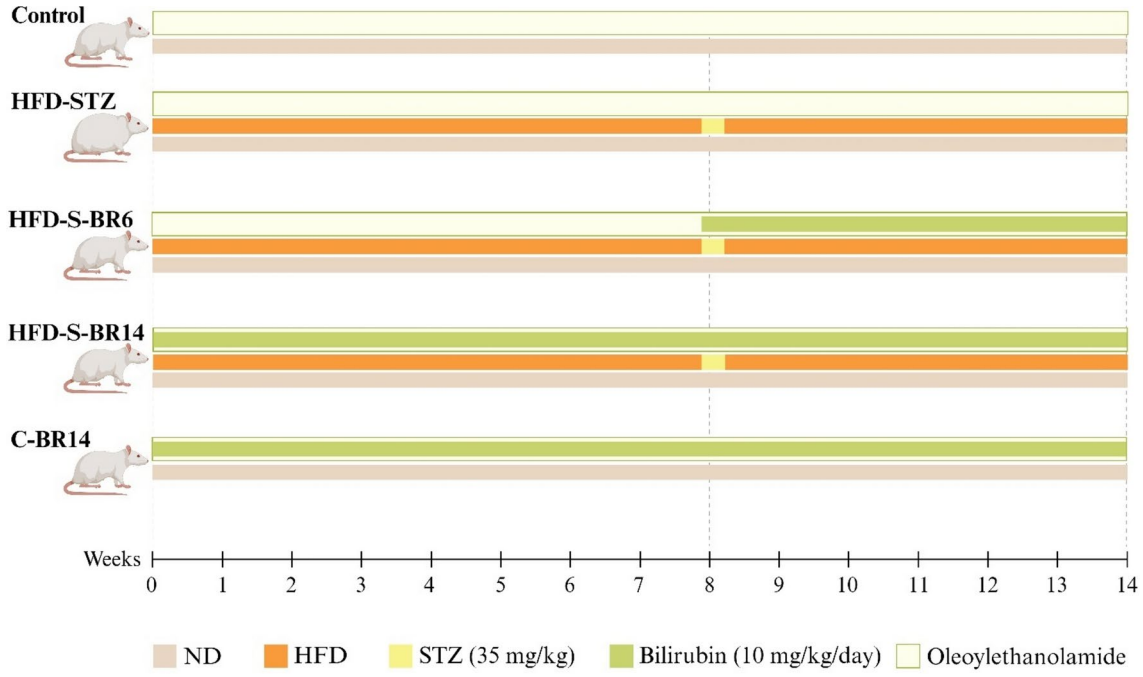

Fig. 1. Schematic figure of the experiment design in rats. Control group: rats receiving a normal diet and treated with oleoylethanolamide for 14 weeks as the vehicle; **HFD-STZ**: Rats receiving high-fat diet (HFD), streptozotocin (STZ), and oleoylethanolamide for 14 weeks; **HFD-S-BR6**: HFD-STZ rats receiving oleoylethanolamide alone for the first 8 weeks and then along with it received bilirubin for the next 6 weeks; **HFD-S-BR14**: HFD-STZ rats treated with bilirubin for 14 weeks; and **C-BR14**: Healthy rats treated with only bilirubin for 14 weeks.

Components of high fat emulsion	Amount
Corn oil (g)	400
Saccharose (g)	150
Total milk powder (g)	80
Cholesterol (g)	100
Sodium deoxycholate (g)	10
Tween 80 (g)	36.4
Propylene glycol (g)	31.1
Vitamin mixture (g)	2.5
Cooking salt (g)	10
Mineral mixture (g)	1.5
Distilled water (ml)	300
Total energy (kcal/l)	4342

Table 1. The composition and caloric content of the high-fat emulsion.

rationale for the 6 week bilirubin treatment period in the HFD-S-BR6 group. Based on prior research and our pilot experiments, it was recommended that treatment commenced following the STZ injection, which occured 8 weeks after dietary manipulation[20]. Non-fasting blood glucose levels were measured two weeks post-STZ injection using a lancet and an Accu-Chek glucometer to evaluate the effects of the treatment. Additionally, the body weight of the animals was assessed on a weekly basis.

At the end of the week 14, after weighing and a 15-h fasting, rats were anesthetized with an intraperitoneal injection of ketamine and xylazine solution (Sigma Aldrich, USA; Cat. No. K113)[38]. In accordance with the guidelines established by the university's ethics committee, each rat was euthanized by placing it in a CO_2 chamber. Subsequently, blood samples were collected from the cardiac cavity. Following the excision and rinsing of the livers with cold saline, both the weight and volume of the livers were promptly measured to determine stereological parameters and the liver index, defined as liver weight divided by the body weight (expressed as a value less than 100). Portions of the liver were then frozen in liquid nitrogen and stored at − 80 °C for subsequent Real-time Quantitative PCR (RT-qPCR) analysis. Additionally, a segment of the tissue samples was excised and preserved in 10% formalin buffer (Merck, Germany; Cat. No. 104002) for stereological and pathological examinations.

GO and KEGG pathway analysis

The enrichment analysis was performed utilizing a variety of bioinformatics tools to elucidate significant biological processes and pathways associated with genes implicated in MAFLD (same as NAFLD). The methodology was structured as follows: initially, a curated set of genes pertinent to MAFLD was entered into the Kyoto Encyclopedia of Genes and Genomes (KEGG) mapper tool, which generated a comprehensive map of the involved genes. The genes of interest were distinctly highlighted to facilitate subsequent analyses (Gene Input and Mapping). Following this, the Enrichr-KG tool was employed to explore the biological processes linked to the input genes. This phase involved querying several databases, including Gene Ontology (GO) for biological processes, Reactome, DisGeNET, KEGG, and WikiPathways (Enrichment Analysis). Subsequently, statistical metrics were computed for each identified biological process and pathway. These metrics included p-values, q-values (adjusted for multiple testing), z-scores, and combined scores to evaluate the significance of the enrichment (statistical evaluation). Eventually, results from the various databases were systematically compiled into tables to enable clear comparisons of the identified biological processes and pathways (Data Compilation).

Biochemical analyses

For biochemical analyses, blood samples were centrifuged at 3000 rpm for 15 min, and the serum fractions were subsequently frozen at − 20 °C. An automated biochemistry analyzer (Prestige 24i, Japan) was utilized to assess serum levels in all rats for the following parameters: blood urea nitrogen (BUN), creatinine (Cr), total cholesterol (TC), triglycerides (TG), low-density lipoprotein (LDL)-cholesterol, high-density lipoprotein (HDL)-cholesterol, alanine aminotransferase (ALT), aspartate aminotransferase (AST), alkaline phosphatase (ALP), total bilirubin (TBIL), and direct bilirubin (DBIL).

mRNA expression status of the target genes

Initially, the frozen liver tissues (50–100 mg) were homogenized using a Potter–Elvehjem homogenizer (Bodine Electric, Chicago, IL, USA) and total RNA was extracted using the YTzol extraction solution (Yekta Tajhiz Azma, Iran; Cat. No. YT9065). In all steps, the samples were put on ice, and centrifugation was at 4 °C. The homogenates were mixed with 1 ml YTzol reagent and incubated for 5 min. Then, 0.2 ml chloroform (Merck, Germany; Cat. No. 107024) was added to the microtube, which was vortexed for 15 s. The mixtures were incubated for 5 min, and centrifugation for phase separation was done at 12,000 RCF for 15 min. Next, 0.4 ml of the aqueous layer was separated, mixed with 0.4 ml isopropanol (Merck, Germany; Cat. No. 109634), and incubated for 15 min. The microtubes underwent centrifugation at 12,000 RCF for 15 min, and the supernatants were cautiously removed. The RNA pellets were rinsed once with 1 ml of 75% ethanol (Merck, Germany; Cat. No. 100983) and then centrifuged at 7500 RCF for 8 min. After the final centrifugation, the ethanol was carefully separated, and

RNA pellets were air-dried. Finally, the RNAs were dissolved in 0.05 ml DEPC-treated water (CinnaGen, Iran; Cat. No. MR8244C) and heated at 55 °C for 10 min[39]. Integrity and purity of the total RNA extracted from the homogenate were assessed using agarose gel electrophoresis and a NanoDrop spectrophotometer. Subsequently, total RNA was reverse-transcribed into complementary DNA (cDNA) utilizing a cDNA synthesis kit (Yekta Tajhiz Azma, Iran; Cat. No. YT4500). RT-qPCR was performed to evaluate the mRNA expression levels of PPAR-α, PGC-1α, SIRT1, NF-κB, TNF-α, IL-6, and IL-1β, with α-actin serving as the housekeeping gene[40]. The primer sequences for the target genes were designed using the Allele ID program (version 7.73), as detailed in Table 2.

RT-qPCR protocol commenced with an initial denaturation step at 95 °C for 10 min, followed by 35 cycles consisting of denaturation at 95 °C for 15 s, annealing at 60 °C for 30 s, and extension at 72 °C for 30 s. This was concluded with a final extension step at 72 °C for 10 min. A no-template control (NTC) using sterile nuclease-free water (ddH2O) was included to ensure the accuracy of expression quantification, which was performed in duplicate for each sample. Relative quantification of gene expression was conducted using the $2^{-\Delta\Delta Ct}$ method, which assesses the difference in cycle threshold (Ct) values (ΔCt) between the reference gene and the target gene[41].

Stereological and histopathological studies

The unbiased stereology was used to evaluate the structural changes related to the liver. In addition to the quantitative exposition of changes, stereological assessments were applied to define the extent of changes.

Estimating the liver volume

Following the cleaning of the livers, their volume (V_{liver}) was determined using the Scherle method[42]. In summary, the liver was suspended with thin threads and placed into a bottle containing regular saline. The weights of the bottle before and after the liver's insertion were recorded. The total liver volume in cubic centimeters (cm^3) was calculated by subtracting the pre-insertion weight from the post-insertion weight, and this value was subsequently divided by the specific gravity of normal saline (1.0048 g/cm^3)[43]. For stereological and histopathological investigations, the orientation method was applied to obtain Isotropic Uniform Random (IUR) sections[44]. As previously stated, we first stored the newly extracted tissues at 4 °C for hematoxylin and eosin (H&E) staining. After that, we left the tissues in formalin fixative for 7 days, changing the fixative solution every 24 and 48 h. The liver tissue samples were fixed in paraffin after the slices and a circle punched out combined were dehydrated using a graded ethanol series. The sections made using a microtome (5 and 25 μm) were then stained with H&E dye. The following formula was used to calculate the rate of tissue volumetric shrinkage[44]:

$$Volume\ shrinkage\ =\ 1-(AA/AB)^{1.5}$$

where "AA" and "AB" were the areas of circular pieces, after and before tissue processing, cutting, and staining, respectively (AB = 4.5 mm). The final volume of the liver was then calculated by the following formula[44]:

$$V_{final\ liver}\ =\ V_{primary}\times(1-Volume\ shrinkage)$$

Estimating the volume density of the liver components

To evaluate the 5-μm sections, a video-microscopy equipment (Nikon, E200, Japan) was utilized. At a final magnification of 770×, a stage micrometer scanned equidistantly along the X and Y axes, examining 8 to 14 tiny fields for each liver sample. The sample section image on the monitor (Fig. 2A) was covered by the point probe,

Gene	Primers	Sequences
PPAR-α	Forward	CGGGTCATACTCGCAGGAAAG
	Reverse	TGGCAGCAGTGGAAGAATCG
PGC-1α	Forward	GCTTGACTGGCGTCATTCA
	Reverse	ACAGAGTCTTGGCTGCACATGT
SIRT1	Forward	TGACCTCCTCATTGTTATTGGG
	Reverse	TCGCCACCTAACCTATGACAC
NF-κB	Forward	CCAGCACCAAGACCGAAGCAA
	Reverse	CCAGCACCAAGACCGAAGCAA
TNF-α	Forward	ACTGAACTTCGGGGTGATCG
	Reverse	GCTTGGTGGTTTGCTACGAC
IL-6	Forward	TGTATGAACAGCGATGATG
	Reverse	AGAAGACCAGAGCAGATT
IL-1β	Forward	CTGTGACTCGTGGGATGATG
	Reverse	AGGGATTTTGTCGTTGCTTG
β-actin	Forward	CACACCCGCCACCAGTTCG
	Reverse	ACCCATTCCCACCATCACACC

Table 2. Primers' sequences.

which had 25 points. The volume density (Vv) of the tissue components, e.g., hepatocytes and sinusoids, was calculated using the point counting method and the following equation[44,45]:

$$V_V = \sum P_{(component)} / \sum P_{(reference)}$$

$$V_{(component)} = V_{V(component)} \times V_{(final\ liver)}$$

where $P_{(component)}$ and $P_{(reference)}$ were total points in the component's profile and the reference space, respectively.

Estimating the number of hepatocytes' nuclei and Kupffer cells

Using tissue sections with a thickness of 25 µm, the "optical dissector method" and the unbiased counting frame at a final magnification of ×1440 were used to determine the number of Kupffer cells and nuclei of hepatocytes (Fig. 2B). Next, a stereological software (StereoLite, SUMS, Shiraz, Iran), microcator (Heidenhain, Germany), and E200 microscope (numerical aperture = 1.30, oil immersion objective 40×) were used. The following formulas were used to determine the numerical density (NV), the total number of hepatocyte nuclei, and the Kupffer cells[46,47]:

$$N_V = \Sigma Q / (\Sigma P \times \Sigma A \times h) \times (t/BA)$$

$$N_{(total)} = N_V \times V_{(final\ liver)}$$

where "ΣQ" describes the number of the cells counted, "ΣA" describes the total areas of unbiased counting frames (the area of each frame is 1205.5 μm^2), "h" is the height of the dissector (15 µm), "t" is the mean section's thickness of all fields assessed by a microcator (~ 22 µm), and "BA" (Block advance) is the section's thickness of the microtome set at 25 µm.

Histopathological scoring

The liver slides were interpreted by a professional pathologist blinded to all clinical data. The pathologist assessed the presence and severity of histopathological changes using NAFLD activity score (NAS)[48]. Based on Table 4, this scoring criteria includes 12 histological parameters in the liver, which provides a standardized system and semi-quantitative grading to evaluate the extent of liver lesions in MAFLD.

Statistical analyses

Each data point was expressed as mean ± SD. The SPSS software (version 24.0) was utilized for statistical analysis, whereas the GraphPad PRISM software (version 9.5.0) was utilized for designing curves and graphs. One-way analysis of variance (ANOVA) and Tukey's post hoc test were used to assess the statistical significance across numerous treatment groups. The effects of treatment × time were examined by using a two-way repeated

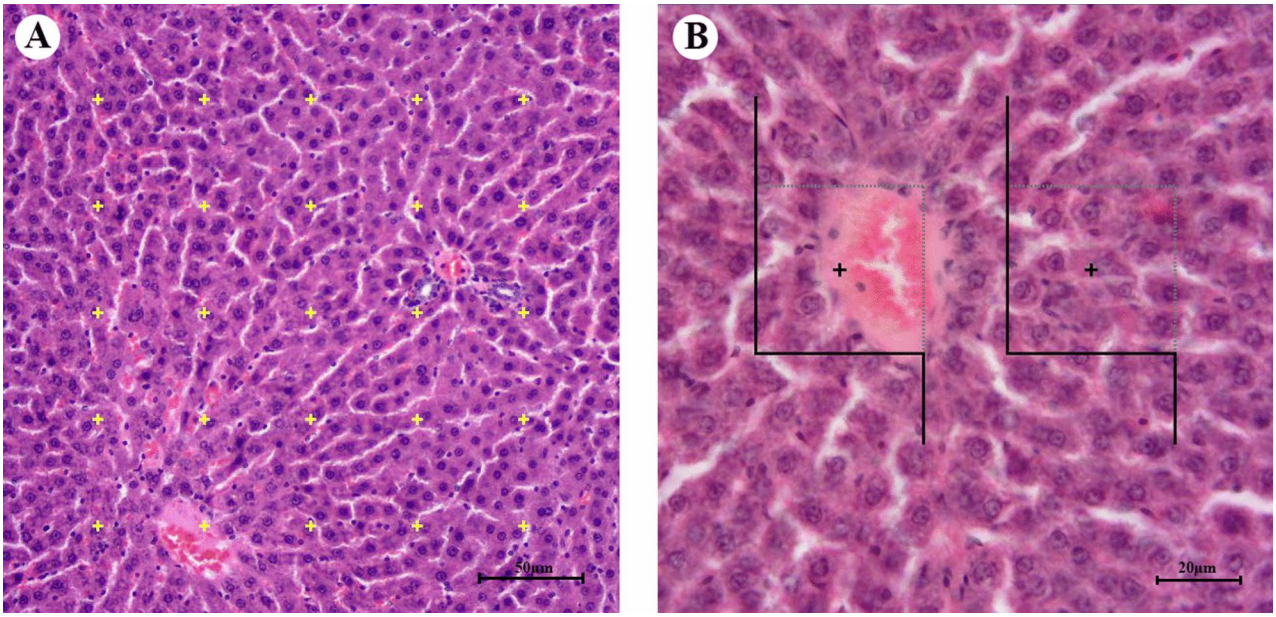

Fig. 2. (**A**) The volume density (Vv) of liver tissue components (i.e., hepatocytes and sinusoids), which was estimated using the point-counting method. (**B**) The optical dissector method was used to indicate the number of hepatocytes' nuclei and Kupffer cells.

measures ANOVA to analyze the changes in the experimental rats' body weight over time. In this investigation, a p-value of less than 0.05 ($p < 0.05$) was deemed statistically significant.

Results

The enrichment analysis yielded several significant biological processes associated with MAFLD

The KEGG enrichment analysis revealed several significantly enriched pathways associated with the DEGs identified in our study. Notably, pathways related to cellular processes such as "apoptosis," "cell cycle," and "metabolic pathways" were among the most enriched (Fig. 3).

Apoptosis Pathway showed a high degree of enrichment ($p < 0.01$), indicating that several DEGs are involved in apoptotic processes, which may suggest a potential mechanism for cell death regulation in response to treatment. Significant enrichment was also observed in cell cycle pathway ($p < 0.05$), highlighting alterations in cell proliferation mechanisms that may contribute to tumor growth dynamics. Metabolic Pathways demonstrated notable enrichment ($p < 0.05$), suggesting that metabolic reprogramming is a critical feature of the biological response observed in our dataset. The graphical representations generated by Enrichr-KG illustrated how specific DEGs mapped onto these pathways, providing insights into their functional roles and interactions within cellular contexts (Fig. 3). Overall, these results underscore the importance of these pathways in understanding the biological implications of the observed gene expression changes.

Biological processes, including negative regulation of lipid storage (GO:0010888), adipocyte differentiation (GO:0045599), and apoptotic process (GO:0043066), and positive regulation of transcription by RNA polymerase II (GO:0045944) (Fig. 4), as well as other pathways identified in KEGG, such as insulin resistance and adipocytokine signaling pathway (Fig. 5) were also found to be correlated with MAFLD but in a non-significant manner. Further enrichment analyses, including Reactome, DisGenNET, and Wikipathway, were performed and their output are available in Supplementary Material 1. For more information on signaling pathways identified in KEGG, also see Supplementary Material 2.

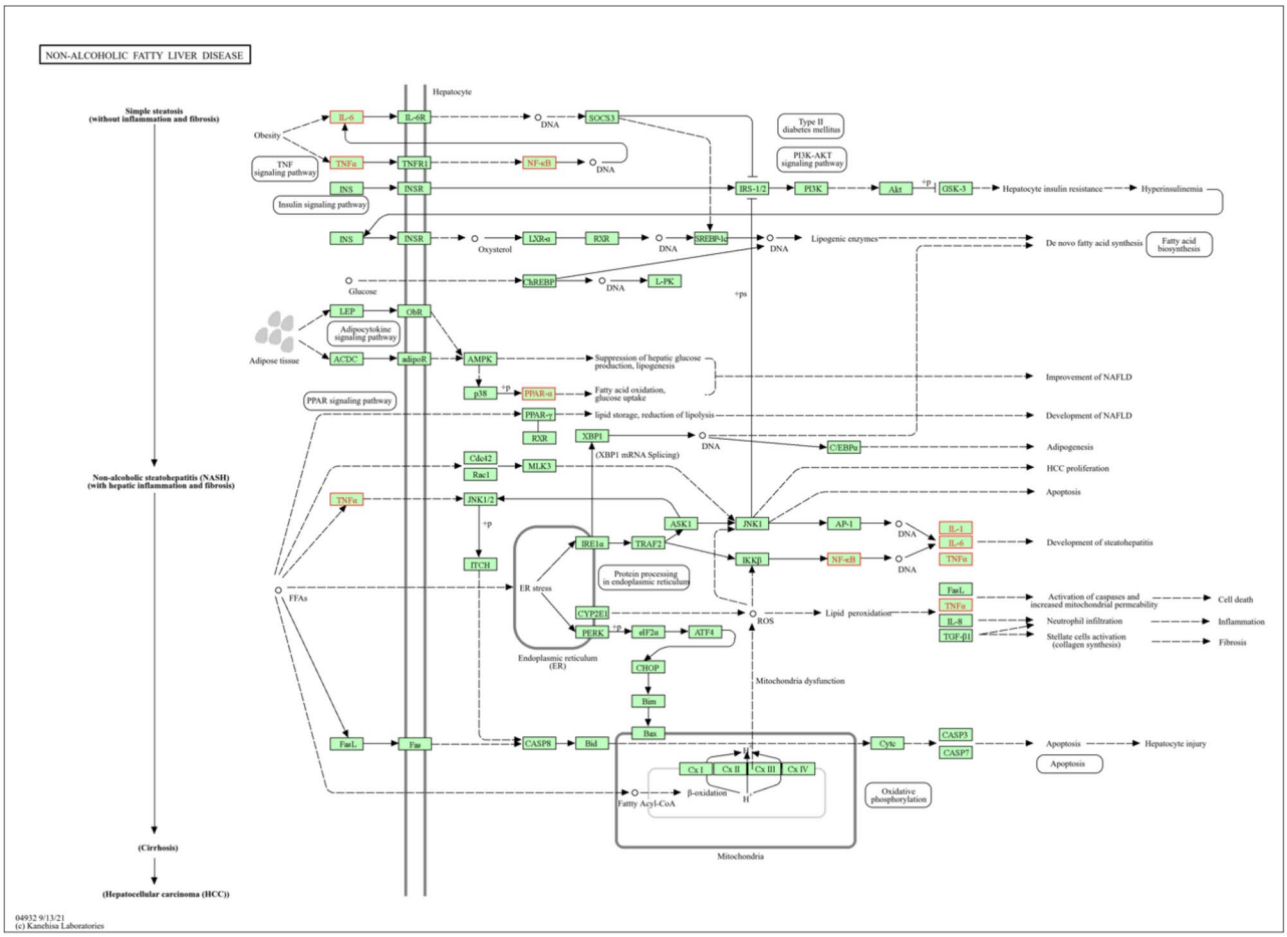

Fig. 3. The general map of involved genes in non-alcoholic fatty liver disease created by KEGG mapper tool. The figure illustrates the results of a pathway enrichment analysis using Enrichr-KG, highlighting significant biological pathways associated with the input gene list.

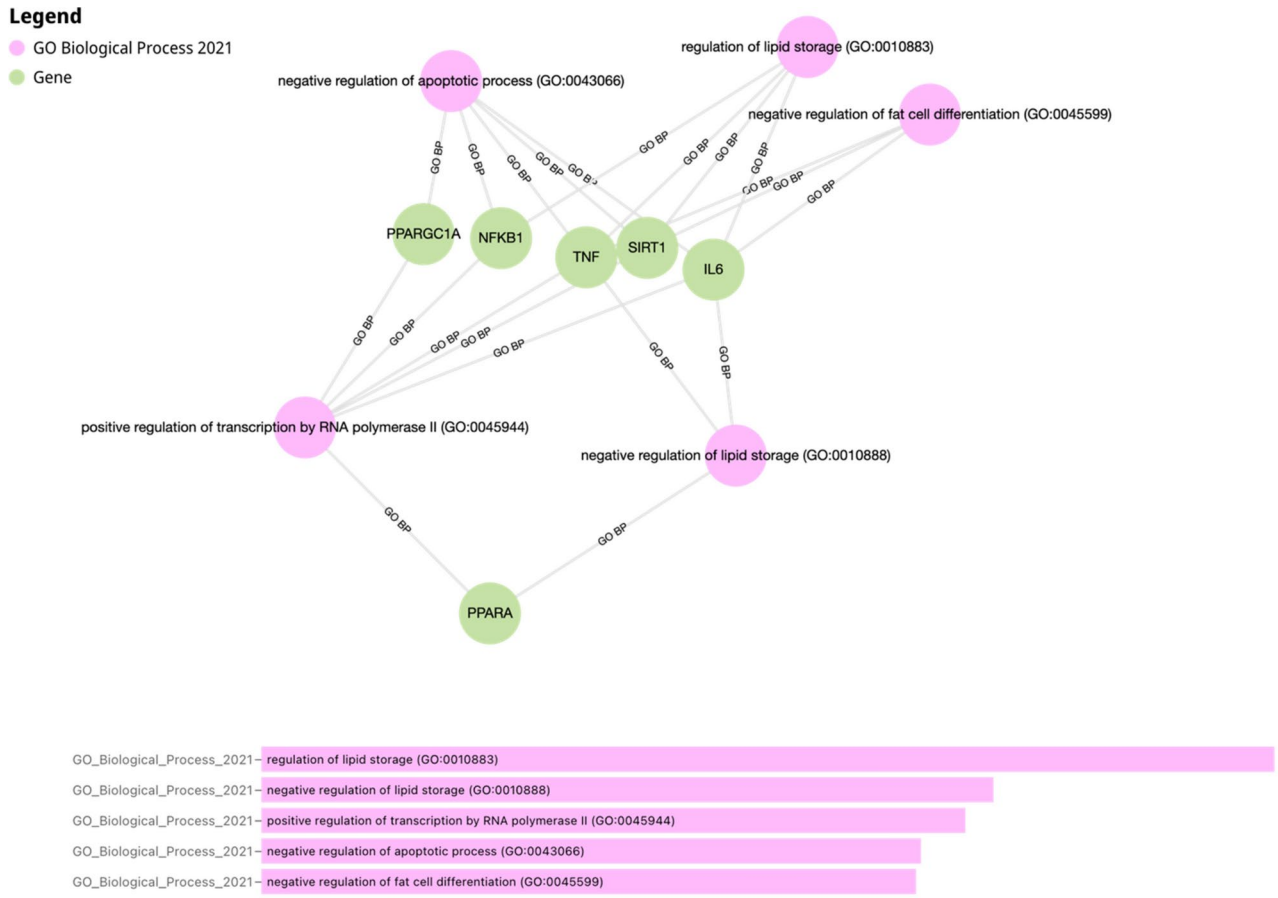

Term	Library	p-value	q-value	z-score	combined ...
regulation of lipid storage (GO:0010883)	GO_Biological_Process_2021	3.8322e-11	2.6979e-8	1480	35490
negative regulation of lipid storage (GO:0010888)	GO_Biological_Process_2021	2.9849e-8	0.000010507	881.3	15270
positive regulation of transcription by RNA polymera...	GO_Biological_Process_2021	5.7994e-8	0.000013609	127	2116
negative regulation of apoptotic process (GO:004306...	GO_Biological_Process_2021	1.6574e-7	0.000021868	101.6	1587
negative regulation of fat cell differentiation (GO:00...	GO_Biological_Process_2021	1.8651e-7	0.000021868	453.6	7029

Fig. 4. A network of genes and biological processes related to MAFLD, as classified by GO biological processes.

Rats' body weight

The results of the two-way repeated measures ANOVA, as illustrated in Fig. 6A, indicate that all HFD groups experienced a time-dependent increase in body weight throughout the duration of the trial ($p < 0.0001$). Compared to the control group, both the HFD-S-BR6 and HFD-STZ groups exhibited significant increases in body weight beginning in the second and fifth weeks, respectively (1.11-fold, $p < 0.01$ and 1.08-fold, $p < 0.05$). In contrast, the increase in body weight was less pronounced in the HFD-S-BR14 group relative to the control group. Notably, the C-BR14 group, which received only bilirubin for 14 weeks, demonstrated a significant weight loss during the final three weeks (weeks 12–14) compared to the control rats (0.91-fold, $p < 0.0001$). The 14th week showed a significant decrease in the average weights of the HFD-STZ, HFD-S-BR6, and HFD-S-BR14 groups (0.86-fold, 0.92-fold, and 0.89-fold respectively), compared to the control group ($p < 0.0001$, $p < 0.001$, and $p < 0.0001$, respectively). These groups had experienced a significant weight loss after the STZ injection.

Figure 6B indicates the variations in weight growth between weeks nine and fourteen. The one-way ANOVA test revealed that the rats in the STZ-treated groups (HFD-STZ, HFD-S-BR6, and HFD-S-BR14) exhibited a transient decrease in body weight (-28.29 ± 3.77 g, -13.5 ± 8.33 g, -3 ± 3.63 g, respectively) in comparison to the rats in the control and C-BR14 groups ($p < 0.0001$). Compared to the HFD-S-BR6 and HFD-S-BR14

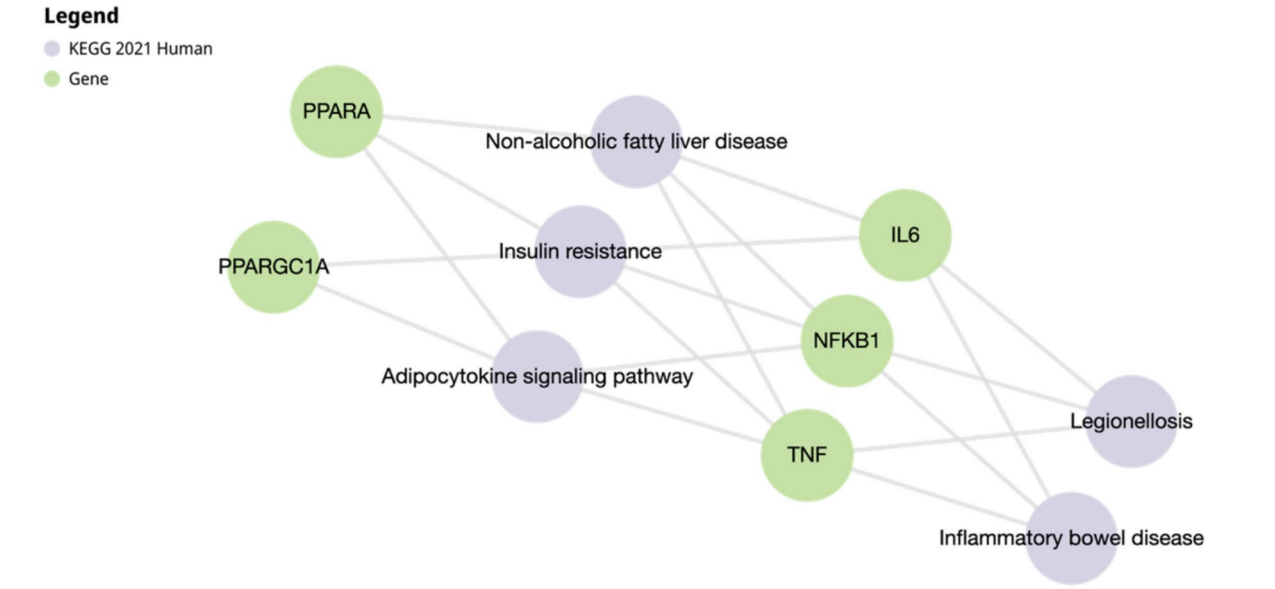

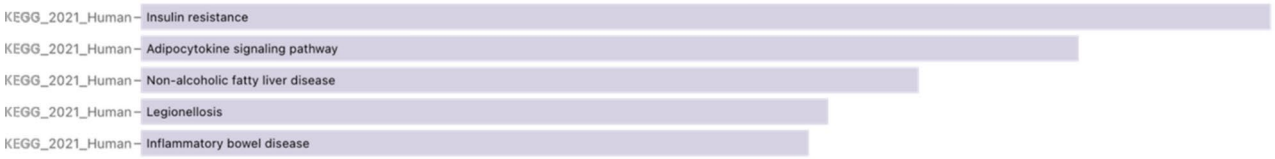

Term	Library	p-value	q-value	z-score	combined ...
Insulin resistance	KEGG_2021_Human	8.7051e-11	9.4015e-9	482.8	11180
Adipocytokine signaling pathway	KEGG_2021_Human	4.5039e-9	2.4321e-7	408.8	7856
Non-alcoholic fatty liver disease	KEGG_2021_Human	1.1927e-7	0.0000042...	175.2	2793
Legionellosis	KEGG_2021_Human	7.6191e-7	0.000020572	276.9	3901
Inflammatory bowel disease	KEGG_2021_Human	0.000001136	0.000024539	241.1	3300

Fig. 5. Other pathways and related disorders identified in KEGG.

groups, the weight loss in the HFD-STZ group was more pronounced ($p < 0.05$ and $p < 0.0001$, respectively), suggesting that the body mass in the bilirubin-treated groups was less decreased. Ultimately, there was no discernible difference between the HFD-S-BR14 and HFD-S-BR6 groups, despite the latter's varying bilirubin administration length.

Liver weight and liver index measurements

The HFD-STZ group's liver weight was 1.21 times greater than that of the control group ($p < 0.01$), but there was no discernible change in the liver weights of the other groups from the control group. Although the liver weights of the HFD-S-BR6 and HFD-S-BR14 groups were lower than those of the HFD-STZ group, the difference was not statistically significant (Fig. 6C).

The liver index was calculated by dividing each rat's liver weight by its total body weight and multiplying the result by 100 (Fig. 6D). Compared to the control group, the liver indices of the HFD-STZ, HFD-S-BR6, and HFD-S-BR14 rats were significantly elevated, with values of 1.4, 1.18, and 1.24-fold increases, respectively

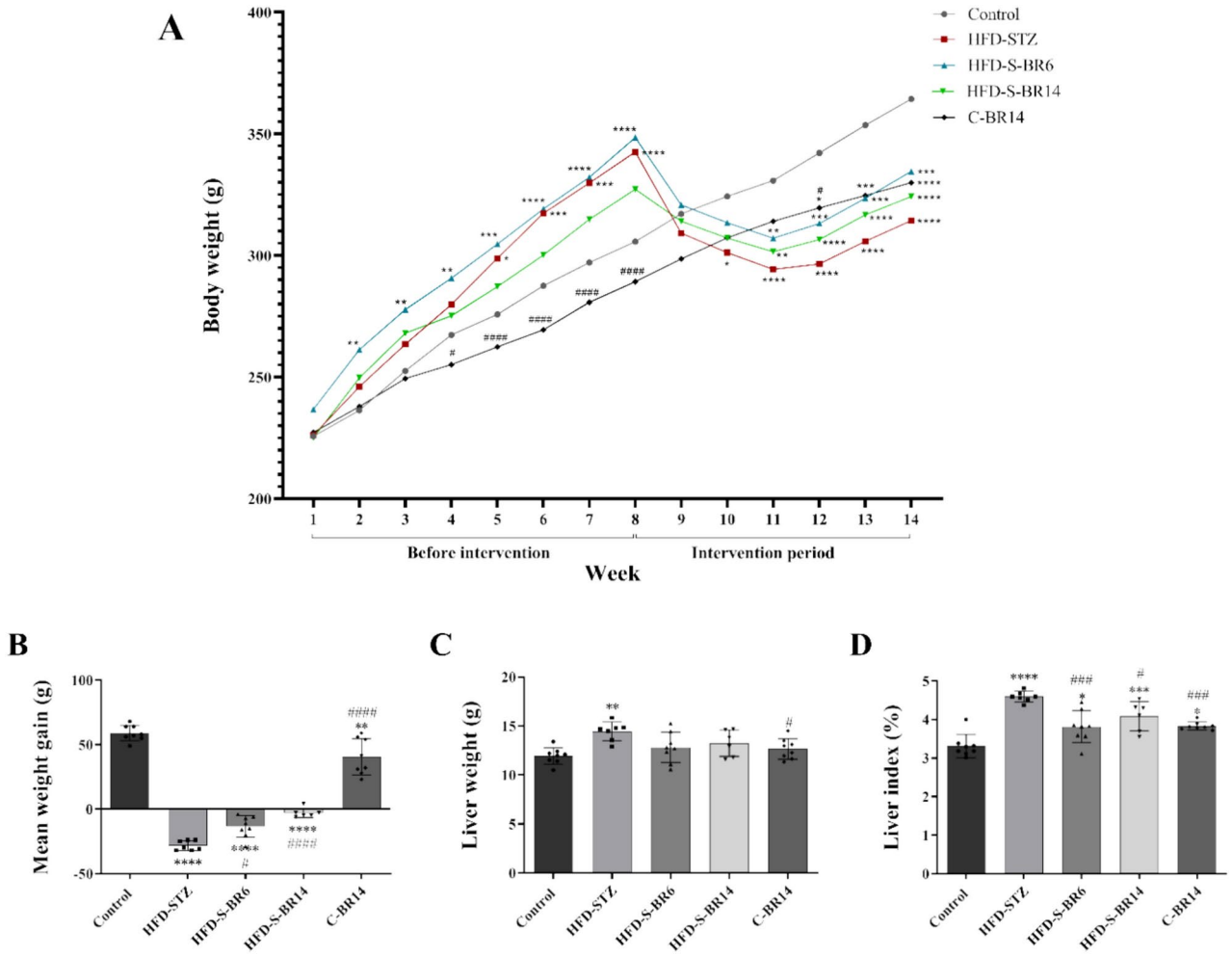

Fig. 6. The assessment of body and liver weight among the studied rats. (**A**) Body weight (g) during 14 weeks of treatment; (**B**) Mean weight gain (g); (**C**) Liver weight (g); and (**D**) Liver index (%). All data have been reported as mean ± SD (n = 6–8). * shows a significant difference between the control group and the other rats, while # indicates a significant difference between the HFD-STZ group and the other rats. Both * or # represent $p < 0.05$, ** or ## represent $p < 0.01$, *** or ### represent $p < 0.001$, and **** or #### represent $p < 0.0001$. **Control group**: Rats receiving a normal diet and treated with oleoylethanolamide for 14 weeks as the vehicle; **HFD-STZ**: Rats receiving high-fat diet (HFD), streptozotocin (STZ), and oleoylethanolamide for 14 weeks; **HFD-S-BR6**: HFD-STZ rats receiving oleoylethanolamide alone for the first 8 weeks and then along with it received bilirubin for the next 6 weeks; **HFD-S-BR14**: HFD-STZ rats treated with bilirubin for 14 weeks; and **C-BR14**: Healthy rats treated with only bilirubin for 14 weeks.

($p < 0.0001$, $p < 0.01$, and $p < 0.001$). Furthermore, the liver indices of the HFD-S-BR6 and HFD-S-BR14 groups were significantly lower than that of the HFD-STZ group, exhibiting reductions of 0.84-fold ($p < 0.001$) and 0.89-fold ($p < 0.05$), respectively.

Effects of bilirubin administration on fasting blood glucose and lipid profile

Serum FBG levels were significantly elevated in the HFD-STZ group compared to the control group, showing a 2.62-fold increase ($p < 0.0001$), as depicted in Fig. 7A. In contrast, bilirubin administration significantly reduced serum FBG levels in the HFD-S-BR6 (0.72-fold) and HFD-S-BR14 (0.63-fold) groups when compared to the HFD-STZ group ($p < 0.0001$).

Also, it is demonstrated that serum levels of TC (1.9-fold), TG (1.94-fold), and LDL-C (3.06-fold) were increased in the HFD-STZ group compared to the control group ($p < 0.0001$) (Fig. 7B–D), while the serum levels of HDL-C were decreased (0.78-fold, $p < 0.001$) (Fig. 7E). Ideally, bilirubin treatment resulted in a significant drop in the serum levels of the aforementioned indices. For example, in the HFD-S-BR6 and HFD-S-BR14 groups, TC (0.74-fold and 0.56-fold), TG (0.79-fold and 0.66-fold), and LDL-C (0.68-fold and 0.55-fold) were all higher than in the HFD-STZ group ($p < 0.0001$). As previously shown, the HDL serum level in the HFD-STZ group was not significantly greater than that of the rats receiving bilirubin, despite the fact that it was significantly lower in the HFD-STZ group compared to the control group. Furthermore, our evaluations did not find any statistically significant changes between the C-BR14 group and the control group (Table 3).

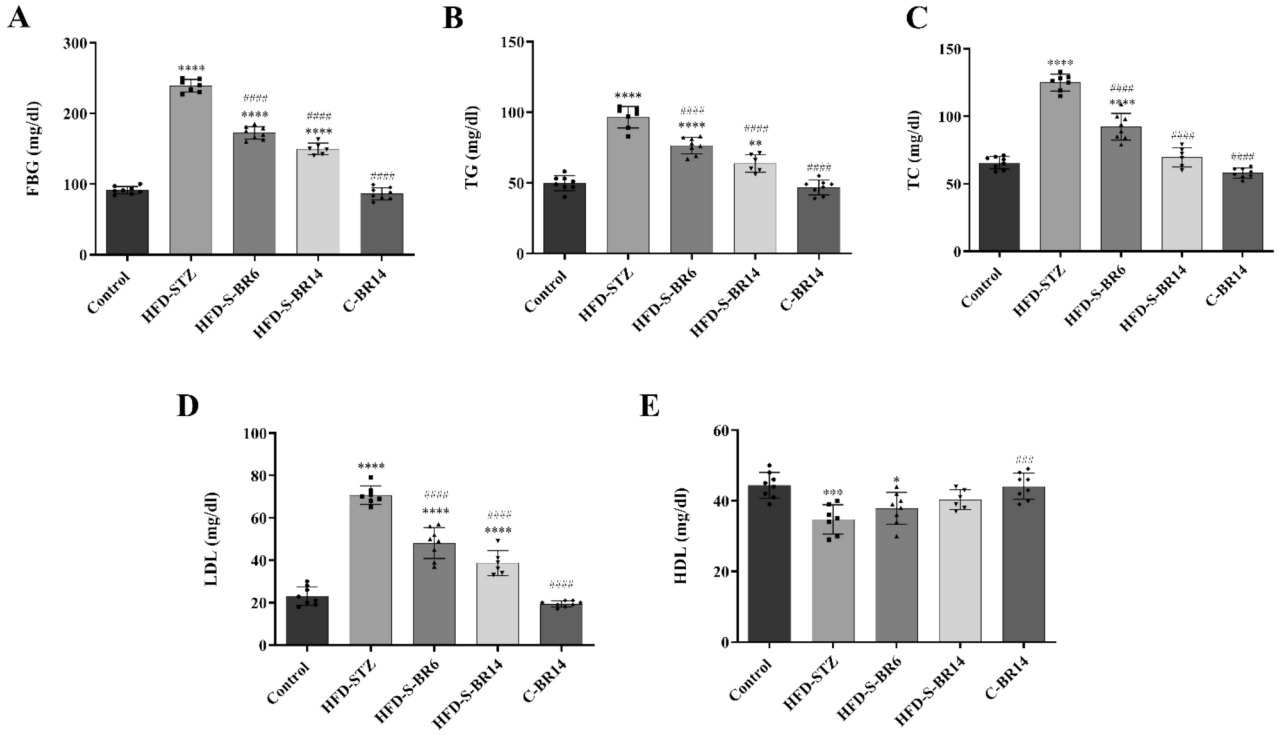

Fig. 7. Serum glucose and lipid profile among different groups of rats. (**A**) FBG; (**B**) TG; (**C**) TC; (**D**) LDL-C; and (**E**) HDL-C. All data have been reported as mean ± SD (n = 6–8). * shows a significant difference between the control group and the other rats, while # indicates a significant difference between the HFD-STZ group and the other rats. Both * or # represent $p < 0.05$, ** or ## represent $p < 0.01$, *** or ### represent $p < 0.001$, and **** or #### represent $p < 0.0001$. Control group: Rats receiving a normal diet and treated with oleoylethanolamide for 14 weeks as the vehicle; HFD-STZ: Rats receiving high-fat diet (HFD), streptozotocin (STZ), and oleoylethanolamide for 14 weeks; HFD-S-BR6: HFD-STZ rats receiving oleoylethanolamide alone for the first 8 weeks and then along with it received bilirubin for the next 6 weeks; HFD-S-BR14: HFD-STZ rats treated with bilirubin for 14 weeks; and C-BR14: Healthy rats treated with only bilirubin for 14 weeks.

Bilirubin administration also has beneficial effects on liver biochemical indices and kidney function

In all groups, variations in the serum levels of liver indices, such as ALT, AST, and ALP, were assessed (Table 3) and (Fig. 8A–C). The HFD-STZ group had higher serum levels of ALT (2.23-fold), AST (2.39-fold), and ALP (1.77-fold) compared to the control group ($p < 0.0001$). On the other front, the injection of bilirubin significantly reduced the serum levels of these three parameters in the HFD-S-BR6 (0.63-fold, 0.67-fold, and 0.65-fold, respectively) and HFD-S-BR14 (0.57-fold, 0.57-fold, and 0.68-fold, respectively) groups compared to the HFD-STZ group ($p < 0.0001$). Furthermore, in those groups receiving bilirubin, total, direct, and indirect bilirubin levels showed a substantial rise ($p < 0.0001$) (Fig. 8D).

Regarding renal function, BUN levels in the serum were significantly higher in HFD-STZ rats than in the control group (1.63-fold, $p < 0.0001$). Additionally, compared to the HFD-STZ group, the BUN levels in the rats treated with bilirubin (HFD-S-BR6 and HFD-S-BR14 groups) significantly decreased (0.82-fold, $p < 0.0001$ and 0.72-fold, $p < 0.0001$, respectively). These outcomes matched the serum creatinine measurements, with the HFD-STZ group exhibiting a statistically significant increase (1.29-fold, $p < 0.0001$) above the control group (Table 3. Furthermore, the HFD-S-BR6 and HFD-S-BR14 groups' serum creatinine levels significantly decreased (0.9-fold, $p < 0.001$, and 0.83-fold, $p < 0.0001$, respectively) in comparison to the HFD-STZ group (Fig. 8E, F).

Bilirubin administration induces the expression of SIRT, PPAR-α, and PGC-1α

The mRNA expression status of SIRT1, PPAR-α, and PGC-1α genes were analyzed, and the results showed that the HFD-STZ group had significantly lower levels of PPAR-α (0.2-fold, $p < 0.001$) and PGC-1α (0.43-fold, $p < 0.01$) mRNA than the control group. Conversely, in comparison to the HFD-STZ group, the HFD-S-BR6 and HFD-S-BR14 groups showed a significant increase in the levels of gene expression for PPAR-α (5.7-fold and 5.9-fold, $p < 0.0001$) and PGC-1α (2.14-fold and 2.05-fold, $p < 0.05$) (Figs. 9A, B).

Furthermore, we discovered that the HFD-STZ (0.29-fold, $p < 0.0001$), HFD-S-BR6 (0.66-fold, $p < 0.05$), and HFD-S-BR14 (0.65-fold, $p < 0.05$) groups had significantly lower SIRT1 mRNA expression levels than the control group. In contrast to the HFD-STZ group, SIRT1 was considerably higher in the HFD-S-BR6 (2.28-fold, $p < 0.05$) and HFD-S-BR14 (2.24-fold, $p < 0.05$) groups (Fig. 9C).

	Control	HFD-STZ	HFD-S-BR6	HFD-S-BR14	C-BR14
FBG (mg/dl)	91.25 ± 5.34	$239.1 \pm 9.1^{****}$	$172.4 \pm 9.04^{****}_{\#\#\#\#}$	$149.7 \pm 8.36^{****}_{\#\#\#\#}$	86.13 ± 8.59
TG (mg/dl)	49.75 ± 5.36	$96.43 \pm 7.66^{****}$	$76.38 \pm 5.9^{****}_{\#\#\#\#}$	$63.67 \pm 6.22^{**}_{\#\#\#\#}$	46.75 ± 5.31
TC (mg/dl)	65.63 ± 4.6	$125 \pm 6.14^{****}$	$92.25 \pm 9.88^{****}_{\#\#\#\#}$	$69.67 \pm 7.2_{\#\#\#\#}$	58 ± 3.66
HDL (mg/dl)	44.38 ± 3.66	$34.71 \pm 4.15^{***}$	$37.88 \pm 4.47^{*}$	40.33 ± 2.8	44.13 ± 3.68
LDL (mg/dl)	23.1 ± 4.42	$70.71 \pm 4.42^{****}$	$48.13 \pm 7.34^{****}_{\#\#\#\#}$	$38.67 \pm 5.89^{****}_{\#\#\#\#}$	19.38 ± 1.41
BUN (mg/dl)	20.7 ± 2.01	$33.83 \pm 1.96^{****}$	$27.66 \pm 1.55^{****}_{\#\#\#\#}$	$24.35 \pm 1.68^{*}_{\#\#\#\#}$	17.88 ± 2.43
Cr (mg/dl)	0.63 ± 0.02	$0.81 \pm 0.056^{****}$	$0.73 \pm 0.038^{****}_{\#\#\#}$	$0.67 \pm 0.029_{\#\#\#\#}$	0.6 ± 0.014
ALT (IU/L)	31 ± 3.59	$69 \pm 4.97^{****}$	$43.25 \pm 6.41^{***}_{\#\#\#\#}$	$39.5 \pm 3.02^{*}_{\#\#\#\#}$	33.63 ± 5.32
AST (IU/L)	44.75 ± 4.89	$107.1 \pm 10.02^{****}$	$71.75 \pm 13.16^{****}_{\#\#\#\#}$	$61.33 \pm 5.99^{*}_{\#\#\#\#}$	47.13 ± 7.62
ALP (IU/L)	476.6 ± 61.8	$842.7 \pm 95.4^{****}$	$544.6 \pm 90.8_{\#\#\#\#}$	$572.7 \pm 51_{\#\#\#\#}$	502.8 ± 50.6
TBIL (mg/dl)	0.09 ± 0.01	0.08 ± 0.008	$0.15 \pm 0.016^{****}_{\#\#\#\#}$	$0.16 \pm 0.009^{****}_{\#\#\#\#}$	$0.176 \pm 0.01^{****}$
DBIL (mg/dl)	0.036 ± 0.007	0.033 ± 0.005	$0.066 \pm 0.012^{****}_{\#\#\#\#}$	$0.073 \pm 0.005^{****}_{\#\#\#\#}$	$0.074 \pm 0.007^{****}$
IBIL (mg/dl)	0.054 ± 0.005	0.047 ± 0.005	$0.084 \pm 0.007^{****}_{\#\#\#\#}$	$0.087 \pm 0.005^{****}_{\#\#\#\#}$	$0.1 \pm 0.014^{****}$

Table 3. Lipid profile and biochemical indices among different groups of rats. All data have been reported as mean ± SD (n = 6–8). * shows a significant difference between the control group and the other rats, while # indicates a significant difference between the HFD-STZ group and the other rats. Both * or # represent $p < 0.05$, ** or ## represent $p < 0.01$, *** or ### represent $p < 0.001$, and **** or #### represent $p < 0.0001$. Control group: Rats receiving a normal diet and treated with oleoylethanolamide for 14 weeks as the vehicle; HFD-STZ: Rats receiving high-fat diet (HFD), streptozotocin (STZ), and oleoylethanolamide for 14 weeks; HFD-S-BR6: HFD-STZ rats receiving oleoylethanolamide alone for the first 8 weeks and then along with it received bilirubin for the next 6 weeks; HFD-S-BR14: HFD-STZ rats treated with bilirubin for 14 weeks; and C-BR14: Healthy rats treated with only bilirubin for 14 weeks.

Bilirubin administration attenuates the expression of NF-κB, TNF-α, IL-6, and IL-1β

The mRNA expression levels of inflammatory NF-κB, TNF-α, Il-6, and Il-1β genes were found to be 3.56-fold, 2.25-fold, 3.22-fold, and 1.79-fold higher in the HFD-STZ group compared to the control group ($p < 0.0001$, $p < 0.01$, $p < 0.0001$, and $p < 0.05$, respectively), as illustrated in Fig. 10A–D. In the HFD-STZ-receiving animals, bilirubin treatment changed the expression of genes involved in inflammation. Thus, in comparison to the HFD-STZ group, the NF-κB (0.59-fold, $p < 0.01$) and Il-6 (0.64-fold, $p < 0.05$) mRNA levels in the HFH-S-BR6 group were significantly lower. Furthermore, compared to the HFD-STZ group, the mRNA expression levels of NF-κB (0.6-fold, $p < 0.01$), TNF-α (0.59-fold, $p < 0.05$), and Il-6 (0.58-fold, $p < 0.01$) were considerably lower in the HFD-S-BR14 group.

Stereological findings: bilirubin treatment affects hepatocytes and the structure of liver tissue

When compared to the control group, the HFD-STZ group's total liver volume rose by 24% ($p < 0.001$) (Fig. 11A). Additionally, the volume of hepatocytes and sinusoids showed increases of 35.7 and 53.6 percent, respectively, above the control group ($p < 0.001$) (Figs. 11B, C). Interestingly, compared to HFD-STZ rats, bilirubin injection decreased the increased total volume of the liver, hepatocytes, and sinusoids in HFD-S-BR6 and HFD-S-BR14 rats, albeit not significantly.

Conversely, Fig. 11D shows that there was a 28.2% increase in hepatocyte nuclei in the HFD-STZ group as compared to the control group ($p < 0.01$). Additionally, 97.9% more Kupffer cells were seen in HFD-STZ mice than in the control group ($p < 0.0001$) (Fig. 11E). However, following bilirubin therapy for 6 and 14 weeks, respectively, the observed rise was considerably reduced to 36.1% and 37.5% in the HFD-S-BR6 and HFD-S-BR14 groups ($p < 0.0001$). Unexpectedly, the number of Kupffer cells increased by 23.3% ($p < 0.05$) in the C-BR14 group, which only received bilirubin for 14 weeks.

Histopathological findings

As provided in Table 4 and Fig. 12, microscopic examinations of the liver sections from the HFD-STZ rats showed severe hepatocellular ballooning and feathery degeneration with microvesicular steatosis, plus severe sinusoidal collapse, as well as a higher number of Kupffer cells compared to the control group, which had liver sections with normal hepatocellular and sinusoidal morphology and no evidence of inflammation. Notably, following the bilirubin treatment, both HFD-S-BR6 and HFD-S-BR14 groups demonstrated a mild-to-moderate hepatocellular ballooning and feathery degeneration, as well as sinusoidal collapse. The hepatocellular and sinusoidal morphology of the C-BR14 group was very similar to the control group. However, a mild increase in the number of Kupffer cells was also observed. All these findings were ultimately confirmed by the H&E staining.

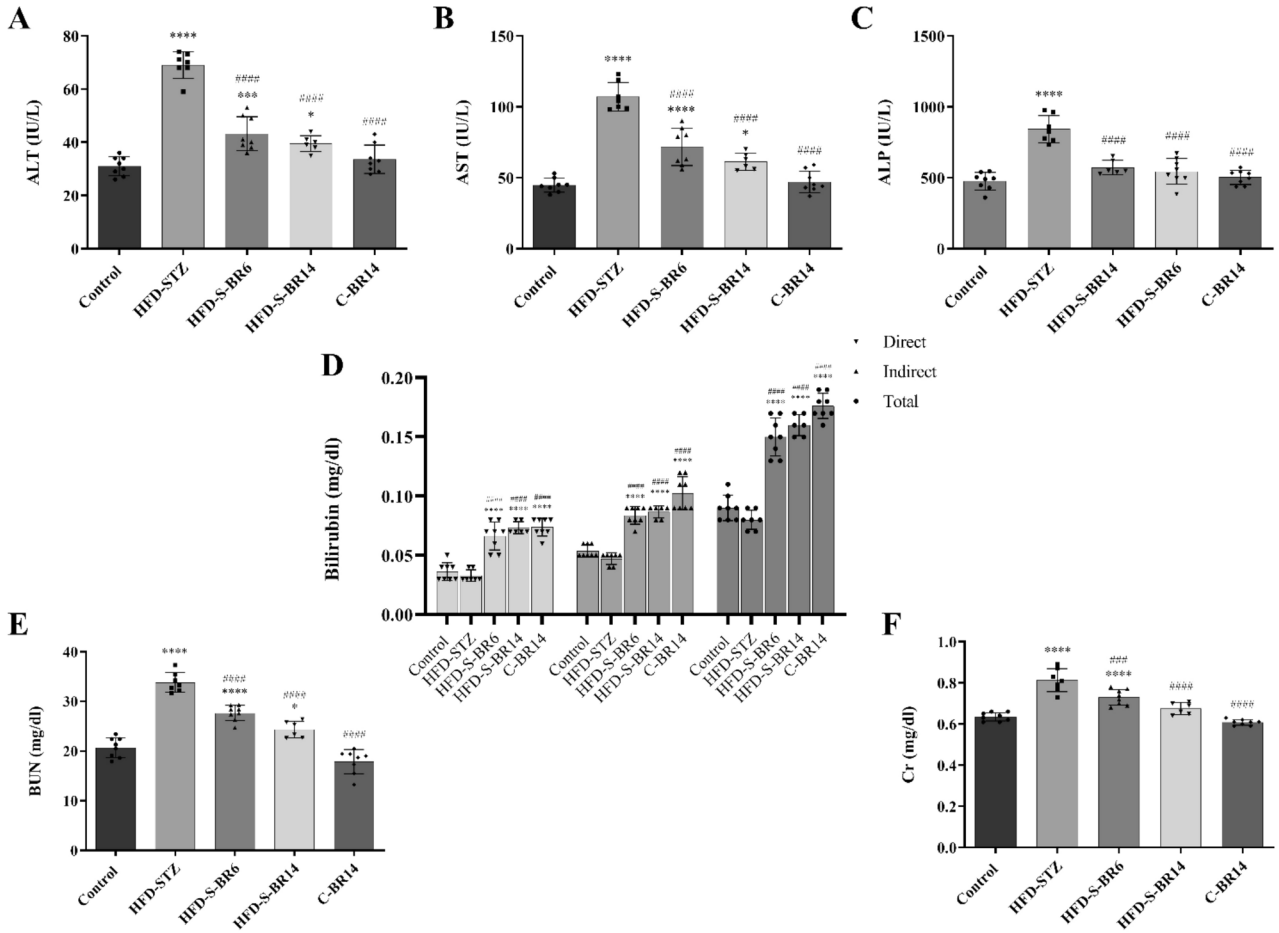

Fig. 8. Serum levels of liver and kidney function indices among different groups of rats. (**A**) ALT; (**B**) AST; (**C**) ALP; (**D**) TBIL, DBIL, and IBIL; (**E**) BUN; and (**F**) Cr. All data have been reported as mean ± SD (n = 6–8). * shows a significant difference between the control group and the other rats, while # indicates a significant difference between the HFD-STZ group and the other rats. Both * or # represent $p < 0.05$, ** or ## represent $p < 0.01$, *** or ### represent $p < 0.001$, and **** or #### represent $p < 0.0001$. Control group: Rats receiving a normal diet and treated with oleoylethanolamide for 14 weeks as the vehicle; HFD-STZ: Rats receiving high-fat diet (HFD), streptozotocin (STZ), and oleoylethanolamide for 14 weeks; HFD-S-BR6: HFD-STZ rats receiving oleoylethanolamide alone for the first 8 weeks and then along with it received bilirubin for the next 6 weeks; HFD-S-BR14: HFD-STZ rats treated with bilirubin for 14 weeks; and C-BR14: Healthy rats treated with only bilirubin for 14 weeks.

Discussion

The results of the enrichment analysis highlight critical biological processes and pathways that may play significant roles in the pathophysiology of MAFLD. The identification of key processes such as lipid storage regulation and transcriptional control suggests potential therapeutic targets for intervention. The extremely low p-values across various pathways indicate a robust association between the input genes and MAFLD-related processes, emphasizing the importance of lipid metabolism in this condition. The high z-scores further reinforce the strength of these associations, suggesting that these pathways are not only statistically significant but also biologically relevant. Moreover, the findings related to insulin resistance and adipocytokine signaling pathways align with existing literature that implicates metabolic dysregulation in MAFLD progression. The connections made through DisGeNET also suggest that MAFLD may share common pathological features with other metabolic disorders, such as diabetes mellitus and alcoholic liver diseases. The current research focused on validating these findings through experimental studies and assessing some of the valuable genes and pathways related to MAFLD.

Hence, our study investigated the impact of bilirubin treatment on the expression of PPAR-α, alongside PGC-1α, SIRT1, and inflammatory cytokines, with a focus on the pathogenesis of MAFLD in rats receiving HFD-STZ. This study has demonstrated that the up-regulation of PPAR-α, PGC-1α, and SIRT1, in conjunction with the down-regulation of NF-κB and pro-inflammatory factors (TNF-α, IL-6, and IL-1β), resulted by bilirubin may have ameliorative effects on MAFLD progression in the HFD-STZ rats. Parenthetically, we used HFD-induced low STZ treated rat model of MAFLD to first examine the effects of unconjugated bilirubin on rats' serum lipid profile, as their HF regimen contained cholesterol along with triglycerides, and second evaluated possible

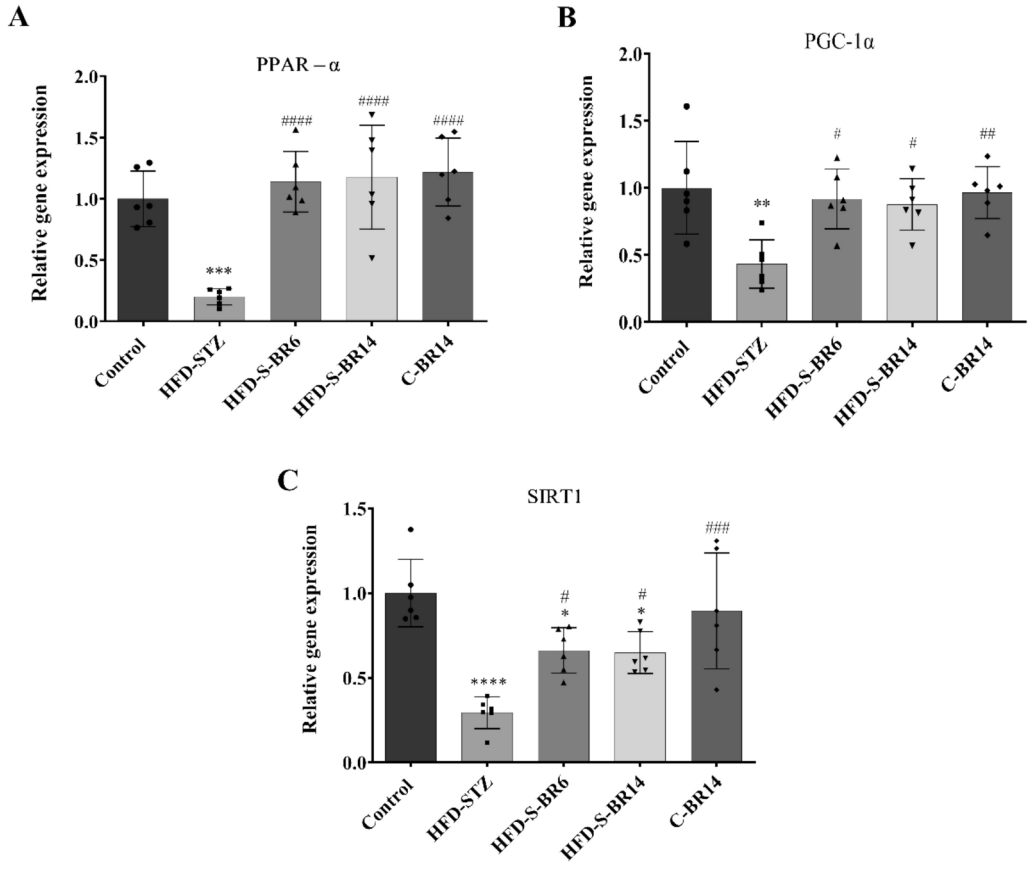

Fig. 9. The relative mRNA expression levels of PPAR-α, SIRT1, and PGC-1α genes in the liver tissue of studied rats. (**A**) PPAR-α, (**B**) SIRT1, and (**C**) PGC-1α. All data have been reported as mean ± SD (n = 6). * shows a significant difference between the control group and the other rats, while # indicates a significant difference between the HFD-STZ group and the other rats. Both * or # represent $p < 0.05$, ** or ## represent $p < 0.01$, *** or ### represent $p < 0.001$, and **** or #### represent $p < 0.0001$. Control group: Rats receiving a normal diet and treated with oleoylethanolamide for 14 weeks as the vehicle; HFD-STZ: Rats receiving high-fat diet (HFD), streptozotocin (STZ), and oleoylethanolamide for 14 weeks; HFD-S-BR6: HFD-STZ rats receiving oleoylethanolamide alone for the first 8 weeks and then along with it received bilirubin for the next 6 weeks; HFD-S-BR14: HFD-STZ rats treated with bilirubin for 14 weeks; and C-BR14: Healthy rats treated with only bilirubin for 14 weeks.

ameliorative effects of bilirubin on FBG levels. Furthermore, previous investigations have demonstrated that NAFLD and T2DM have reciprocal interactions and can provide a valid MAFLD model for multiple analyses when employed simultaneously[1,49].

In this era, growing evidence has suggested that PPAR-α activation provides several metabolic benefits for controlling lipid homeostasis. Interestingly, PPAR-α can increase liver fat metabolism and remove fatty acids as the substrates for lipid peroxidation. This effect is highly important enough in the prevention of MAFLD[50,51]. Consistently, it has been reported that the activation of PPAR-α with different PPAR-α agonists could improve steatosis and inflammation[52]. As an example, it has been shown that mice with PPAR-α KO developed hepatic steatosis and hypertriglyceridemia, and were unable to induce ketogenesis in response to conditions in which fatty acids were used as the main source of energy, like diabetes and the fasting state[53,54].

Furthermore, the effects of SIRT1 on fatty acid metabolism should also be borne in mind. In this regard, a study illustrated that hepatocyte-specific deletion of SIRT1 in mice not only resulted in a higher level of cholesterol when fed HFD, but also resulted in increased cholesterol when fed HFD without cholesterol. These observations highlight the role of SIRT1 in the regulation of de novo synthesis of liver cholesterol[55]. Recent evidence indicates that SIRT1 can also regulate PPAR-α activity by deacetylation, and its loss of function results in decreased expression of PPAR-α target genes involved in fatty acid oxidation[56,57]. On the other hand, PPAR-α could attach to the upstream of SIRT1 promoter by PPREs and induce its gene expression as a transcription factor. Therefore, there exists a positive feedback between PPAR-α and SIRT1[55,58]. A study demonstrated that the deletion of SIRT1 in hepatocytes leads to increase in PGC-1α acetylation levels disrupted PPAR-α signaling followed by a decrease in fatty acid β-oxidation, hepatic steatosis, liver inflammation, and ER stress[55,59]. So, the activation of SIRT1 in association with PGC-1α and PPAR-α controls the expression of target genes involved in lipid metabolism[59] and it has also been shown that using PPAR-α activators could also increase SIRT1 expression[56].

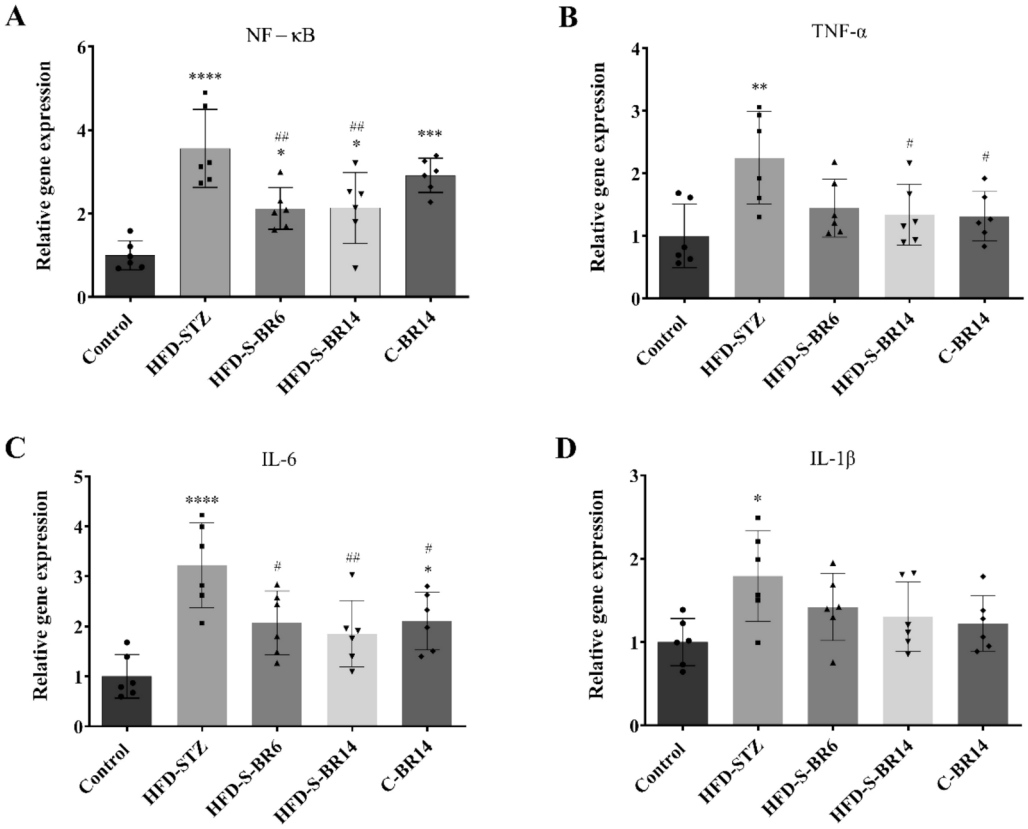

Fig. 10. The relative mRNA expression levels of inflammation-related genes in the liver tissue of studied rats. (**A**) NF-κB, (**B**) TNF-α, (**C**) IL-6, and (**D**) IL-1β. All data have been reported as mean ± SD (n = 6). * shows a significant difference between the control group and the other rats, while # indicates a significant difference between the HFD-STZ group and the other rats. Both * or # represent $p < 0.05$, ** or ## represent $p < 0.01$, *** or ### represent $p < 0.001$, and **** or #### represent $p < 0.0001$. Control group: Rats receiving a normal diet and treated with oleoylethanolamide for 14 weeks as the vehicle; HFD-STZ: Rats receiving high-fat diet (HFD), streptozotocin (STZ), and oleoylethanolamide for 14 weeks; HFD-S-BR6: HFD-STZ rats receiving oleoylethanolamide alone for the first 8 weeks and then along with it received bilirubin for the next 6 weeks; HFD-S-BR14: HFD-STZ rats treated with bilirubin for 14 weeks; and C-BR14: Healthy rats treated with only bilirubin for 14 weeks.

A better understanding of whether the prevention of MAFLD by PPAR-α ligands or SIRT1 activators may help reduce intrahepatic fat or not could be highly valuable in designing potential therapeutic tools. In this regard, it was previously reported that bilirubin had beneficial effects in dealing with inflammatory diseases such as NAFLD, as well as MAFLD due to its antioxidant effects[25,28,60,61]. Here, our study also showed that the HFD-STZ rats treated with bilirubin had significantly higher expression levels of PPAR-α, SIRT1, and PGC-1α compared to the rats that only received HFD-STZ. Indeed, it seems that bilirubin can stimulate PPAR-α, SIRT1, and PGC-1α expression, and it can be deduced that there is a positive feedback between these three factors[55,58]. According to some theories, bilirubin itself may have a new role as PPAR-α's ligand. Bilirubin can bind to PPAR-α directly and boost its transcriptional activity, which in turn causes the target genes for lipid oxidation to be up-regulated. It could account for the shielding effects of a mild elevation in plasma bilirubin levels against the development of hepatic steatosis and other cardiometabolic disorders seen in Gilbert's syndrome patients[30,31,60].

In the current assessment, we found that bilirubin treatment dramatically lowered liver indices, such as ALT, AST, and ALP, as well as FBG, TG, TC, and LDL-C levels in the HFD-STZ group. These outcomes were consistent with other studies that demonstrated that bilirubin's antioxidant qualities led to a significant reduction in the levels of FBG, ALT, and AST in PPAR-α KO HFD-mice after a seven-day treatment[60]. Also, another possible explanation might be attributed to the activation of PPAR-α due to the direct binding of bilirubin and the induction of fibroblast growth factor 21 (FGF21), which is known to decrease blood levels of glucose and lipids[60]. The bilirubin-mediated up-regulation and activation of PPAR-α can also reduce the triglycerides content by stimulating the breakdown of hepatic fatty acids, and this causes the liver to be depleted of lipid sources[32,62].

As the other outcome of our study, NF-kB, TNF-α, IL-6, and IL-1β were found to be down-modulated in HFD-STZ rats treated with bilirubin compared to those that only received HFD-STZ, and this was in parallel to a lower number of Kupffer cells, which was apparent after bilirubin administration, confirming the possible anti-inflammatory effects of bilirubin. Remarkably, recent studies have shown that the inflammatory response and energy metabolism are related to each other through a close interaction between NF-kB and SIRT1

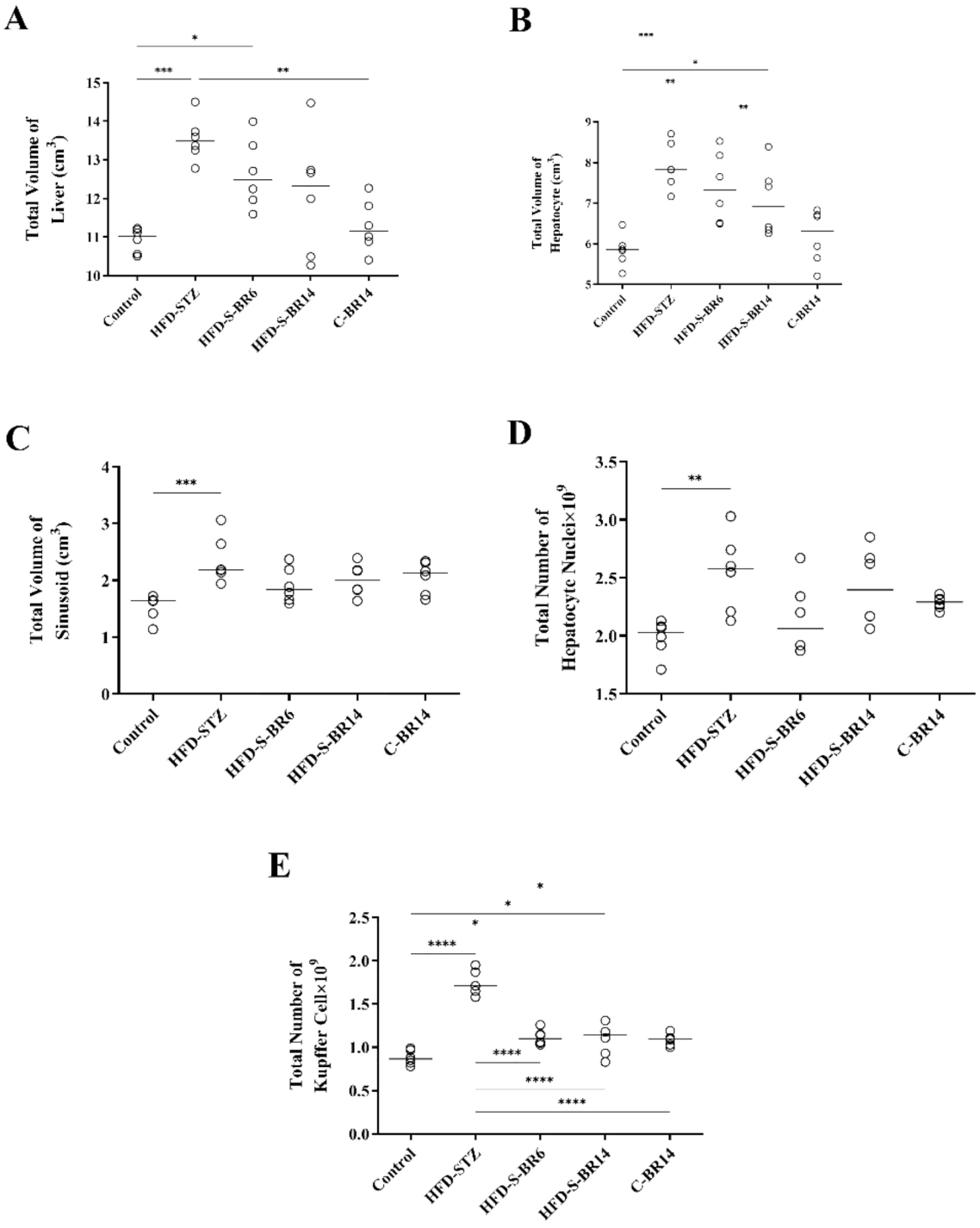

Fig. 11. The quantitative stereological parameters of the liver. (**A**) total volume of the liver (cm^3); (**B**) total volume of hepatocytes (cm^3); (**C**) total volume of sinusoids (cm^3); (**D**) total number of hepatocytes' nuclei; and (**E**) total number of Kupffer cells. All data have been reported as mean ± SD (n = 6). * shows a significant difference between the control group and the HFD-STZ with the other rats. * represent $p < 0.05$, ** represent $p < 0.01$, *** represent $p < 0.001$, and **** represent $p < 0.0001$. Control group: Rats receiving a normal diet and treated with oleoylethanolamide for 14 weeks as the vehicle; HFD-STZ: Rats receiving high-fat diet (HFD), streptozotocin (STZ), and oleoylethanolamide for 14 weeks; HFD-S-BR6: HFD-STZ rats receiving oleoylethanolamide alone for the first 8 weeks and then along with it received bilirubin for the next 6 weeks; HFD-S-BR14: HFD-STZ rats treated with bilirubin for 14 weeks; and C-BR14: Healthy rats treated with only bilirubin for 14 weeks.

Histological parameter	Control	HFD-STZ	HFD-S-BR6	HFD-S-BR14	C-BR14
Steatosis grade	0	1	1	0	0
3: > 66%					
2: 34–66%					
1: 5–33%					
0: < 5%					
Steatosis location	3	1	1	3	3
1: Zone 1					
2: Zone 3					
3: Azonal					
4: Panacinar					
Microvesicular fatty change	0	1	1	0	0
0: Absent					
1: Present					
Fibrosis	0	0	0	0	0
0: None					
1A: Mild, zone 3, perisinusoidal					
1B: Moderate, zone 3, perisinusoidal					
1C: Portal/periportal					
2: Perisinusoidal and portal/periportal					
3: Bridging fibrosis					
4: Cirrhosis					
Lobular inflammation	0	1	0	0	0
0: 0/200×					
1: 1/200×					
2: 2–4/200×					
3: 5/200×					
Microgranuloma	0	0	0	0	0
0: Absent					
1: Present					
Lipogranuloma	0	0	0	0	0
0: Absent					
1: Present					
Portal inflammation	0	1	0	1	0
0: None to minimal					
1: Greater than minimal					
Ballooning change	0	2	2	2	1
0: None					
1: Few					
2: Many					
Acidophilic body	0	0	0	0	0
0: None to rare					
1: Many					
Mallory body	0	0	0	0	0
0: None to rare					
1: Many					
Glycogenated nuclei	0	0	0	0	0
0: None to rare					
1: Many					

Table 4. Histopathological scoring of the liver biopsy in different groups of rats (NAFLD activity score (NAS) system).

transductions[15]. NF-κB signaling is a key regulator of inflammation, whereas SIRT1 is an important regulator of energy metabolism and cell survival[15]. Nevertheless, NF-κB signaling can change its function to also control the energy homeostasis during inflammation, while growing evidence has confirmed that SIRT1 can inhibit NF-κB by deacetylating its p65 subunit[63]. In addition, SIRT1 can increase histones deacetylation in the promotors of TNF-α, IL-6, and IL-1β and suppressing their expression[63]. SIRT1 has also been shown to stimulate energy

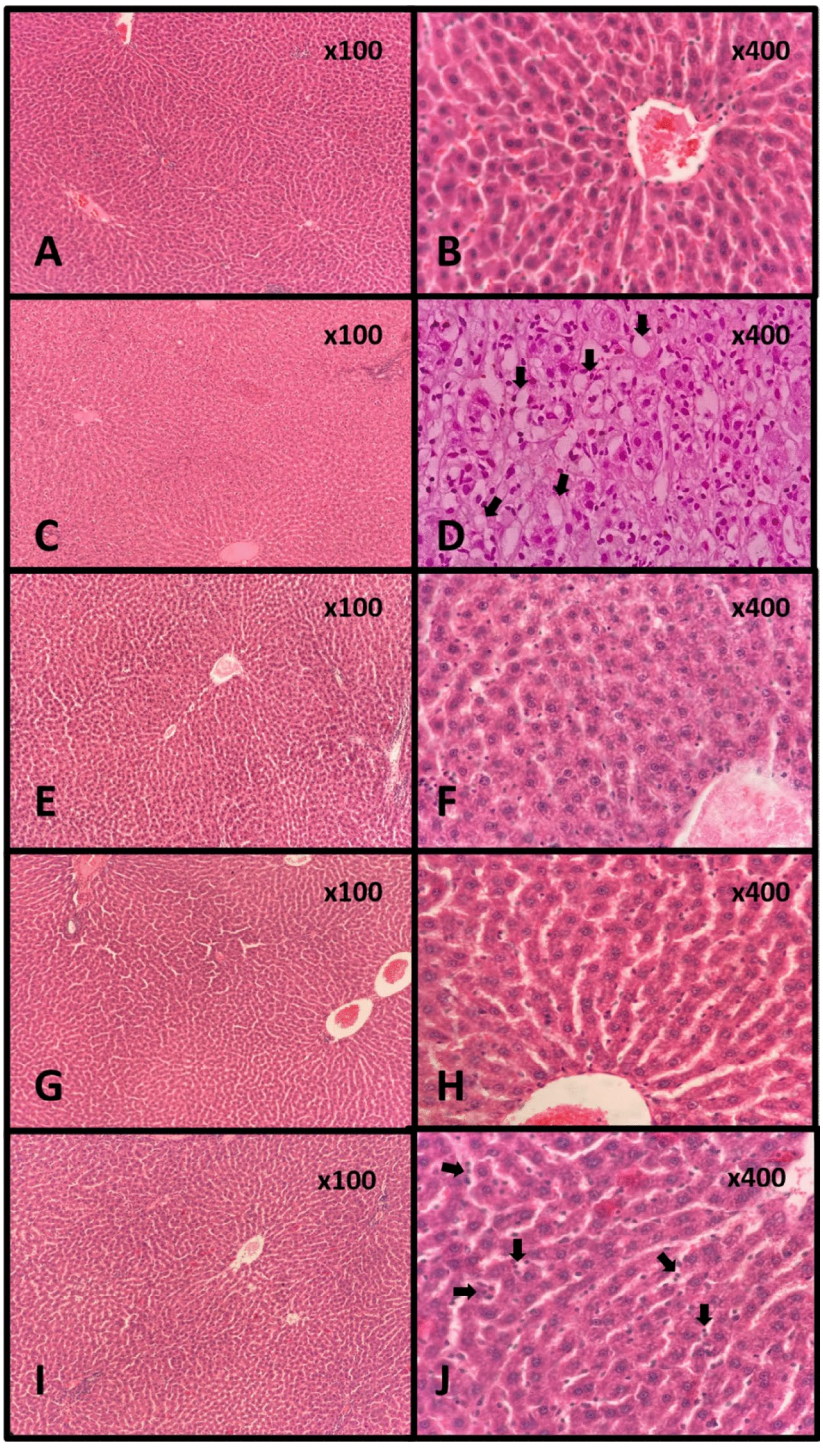

Fig. 12. Microscopic histopathological assessments of the liver in different groups. (**A**) (X100, H&E staining) and (**B**) (X400, H&E staining): Histopathological sections of the control group show normal hepatocellular and sinusoidal architecture and morphology without any inflammation. (**C**) (X100, H&E staining) and (**D**) (X400, H&E staining): Histopathological sections of the HFD-STZ group show moderate hepatocellular ballooning, feathery degeneration with microvesicular steatosis (Arrows), and severe sinusoidal collapse. (**E**) (X100, H&E staining) and (**F**) (X400, H&E staining): Histopathological sections of the HFD-S-BR6 group show moderate hepatocellular ballooning, feathery degeneration, and mild sinusoidal collapse. (**G**) (X100, H&E staining) and (**H**) (X400, H&E staining): Histopathological sections of the HFD-S-BR14 group show mild hepatocellular ballooning, feathery degeneration, and mild sinusoidal collapse. (**I**) (X100, H&E staining) and (**J**) (X400, H&E staining): Histopathological sections of the C-BR14 group show near normal hepatocellular and sinusoidal architecture and morphology. Arrows show Kupffer cells in sinusoids which show mild increase in their quantity.

production through the activation of PPAR-α and PGC-1α, and these factors can also inhibit the NF-κB and suppress the inflammatory response[56,64]. In parenthesis, the promoter of SIRT1 contains binding sites for the p65 subunit of NF-κB as a transcription factor, and thus the expression of SIRT1 could be enhanced by NF-κB[65,66].

Considering the above-stated information, PPAR-α reduces inflammation by forming inhibitory complexes with NF-κB; in detail, PPAR-α can block the nuclear translocation of the NF-κB[67]. Furthermore, lipid mediators, such as omega-3 fatty acids, which are in close association with PPAR-α, also play a key role in suppressing inflammation through the inhibition of NF-κB[64]. The formation of PPAR-α and p65 complex could be stimulated by SIRT1, and consequently, the following inflammatory response and undesired metabolic effects are inhibited as well[63]. Last but not least, the overexpressed NF-κB and subsequent inflammatory responses disrupt SIRT1 and PPAR-α-mediated metabolism and cause metabolic defects[64]. In this regard, some studies highlighted that inflammatory cytokines reduce PPAR-α mRNA expression at the level of gene transcription in fatty liver disease[62]. Another point worth mentioning is the higher gene expression of NF-κB observed in C-BR14 rats, as healthy rats treated with only bilirubin compared to the control group. Our logical reasoning here is the toxic effects of high doses of bilirubin in healthy rats, which was also reported in our previous study[20]. NF-kB mediates the cascade bringing about the activation of Kupffer cells by regulating the transcription of downstream cytokines[68]. Therefore, an increase in the expression levels of NF-κB in the C-BR14 group also elevated the number of Kupffer cells.

To confirm the previously mentioned findings, stereological indices, such as the liver's total volume, hepatocytes, and sinusoids as well as histopathological alterations of the rats' liver were also assessed, experimentally. We recognized that HFD-STZ rats receiving bilirubin had lower total volumes of the liver and sinusoids compared to those only received HFD-STZ. To be noted, sinusoids are responsible for controlling the blood flow to hepatocytes, particularly during liver regeneration[69,70]. However, during HFD treatment, an increase was observed in the volume of sinusoids, which could be explained as the consequence of dilatation, followed by hypoxia and ischemia[71,72]. Inflammation was the other outcome of prolonged HFD treatment, which exacerbated liver failure and hepatocellular degeneration, leading to an increase in the liver's total volume[73,74]. Noteworthy, all these observations were desirably improved after bilirubin administration. We also reported an increase in the number of Kupffer cells as a marker indicating the presence of inflammation in the HFD-STZ rats compared to the control group. Kupffer cell activation generates several inflammatory cytokines, such as TNF-α, IL-6, and IL-1β, which ultimately results in the development of hepatic steatosis and chronic liver inflammation[75,76]. Based on previous studies, we expected a decrease to occur in the total number of hepatocytes in the HFD rats in contrast to the control group, which might be explained by attributing to this fact that the number of binucleated hepatocytes is significantly increased in MAFLD concurrent with the disease progression as a result of a compensatory response to the decreased number of hepatocytes due to necrotic alterations[71]. Here we estimated the total number of hepatocytes' nuclei regardless of whether they are uninucleate or binucleated, and this might account for the observed increase in the number of hepatocytes in HFD rats. As ultimately expected, there was severe hepatocellular steatosis in rats receiving the HFD-STZ regimen in line with previous analyses, which was due to the increased hepatic fat accumulation and the development of MAFLD in rats[71,72]. It is interesting to note that our research revealed that bilirubin therapy significantly reduced inflammation, steatosis, and hepatocellular ballooning in addition to improving the overall morphology of the livers of HFD-STZ rats. These results were in line with a study by Hinds et al. that found that in HFD-induced hepatic steatosis, slightly raised plasma bilirubin reduces inflammation and hepatic lipid buildup[77,78]. What could be deduced here is the protective role of bilirubin in preventing intrahepatic lipid accumulation, hepatocyte damages, inflammation, and the progression of hepatic injury from MAFLD to MASH, and these were also in parallel with the findings of gene expression.

Hence, it seems plausible that bilirubin has the ability to stimulate PPAR-α and/or SIRT1 and create a positive feedback loop between them, where their pharmacological activation might be central to MAFLD prevention. In summary, therapeutic strategies that can simultaneously modulate SIRT1, PPAR-α, and NF-κB are of high importance for the treatment of inflammatory hepatic diseases, especially MAFLD. Thus, it seems that bilirubin administration regulates these key factors and alters the expression of their downstream targets in a protective and anti-inflammatory manner.

Together, we acknowledge the necessity for further studies in understanding the exact mechanistic links between bilirubin and key pathways within our studied model. It is worth noting that we streamlined our discussion and introduced additional approaches to comprehensively address our findings and suggest potential areas for future research. However, it is crucial to emphasize the need for future research to fully elucidate these suggested relationships.

Conclusion

From the current investigation, it can be concluded that bilirubin has potential protective and ameliorative effects against MAFLD, particularly by affecting signaling molecules at the gene expression levels, improving biochemical parameters and liver indices, as well as controlling inflammation. Moreover, it became obvious that bilirubin administration could ameliorate structural changes in the rats' livers receiving HFD. Together, our study unveiled the potent role of bilirubin as a promising therapeutic agent against MAFLD. However, it acknowledges some limitations as follows. While we achieved valuable and significant results regarding the expression of SIRT1, PGC-1α, PPAR-α, and NF-κB genes following bilirubin treatment in our MAFLD model, assessing the protein expression levels encoded by these genes could undoubtedly have provided more comprehensive information at the translational level, which unfortunately was not possible due to limitations in our study. Additionally, assessing post-translational modifications (PTMs) could have provided insights beyond translation. This information could have been used to make more accurate predictions about the mechanistic links between bilirubin and the pathogenesis of this MAFLD model. However, due to technical limitations and

resource constraints, we were unable to perform these analyses, as well. To compensate for the lack of protein expression and PTM data, we made extensive efforts to validate our findings using histological and pathological examinations. These analyses provided valuable information about the structural and morphological changes induced by bilirubin treatment in the liver tissue. In future studies, we plan to expand our investigations by measuring the expression of a network of genes downstream of the corresponding genes. This will provide a broader perspective on the molecular mechanisms underlying the protective effects of bilirubin in MAFLD. We acknowledge the limitations of our study in not assessing protein expression and PTMs but we believe that our findings, combined with the planned future studies, will contribute to a more comprehensive understanding of the role of bilirubin in MAFLD pathogenesis.

Data availability

All datasets analyzed during the current study are available from the corresponding author on reasonable requests.

Received: 5 August 2024; Accepted: 15 November 2024
Published online: 25 November 2024

References

1. García-Compeán, D. & Jiménez-Rodríguez, A. R. NAFLD vs MAFLD. The evidence-based debate has come. Time to change?. *Ann. Hepatol.* **27**, 100765 (2022).
2. Han, J. H., Park, M. H. & Myung, C. S. *Garcinia cambogia* ameliorates non-alcoholic fatty liver disease by inhibiting oxidative stress-mediated steatosis and apoptosis through NRF2-ARE activation. *Antioxidants* **10**, 1226 (2021).
3. Ebrahimi, R. et al. Low level of adiponectin predicts the development of nonalcoholic fatty liver disease: is it irrespective to visceral adiposity index, visceral adipose tissue thickness and other obesity indices?. *Arch. Physiol. Biochem.* **128**, 24–31 (2022).
4. Wang, Q., Zhang, Y., Lu, R., Zhao, Q. & Gao, Y. The multiple mechanisms and therapeutic significance of rutin in metabolic dysfunction-associated fatty liver disease (MAFLD). *Fitoterapia* **178**, 106178 (2024).
5. Dynka, D. et al. Beneficial effects of the ketogenic diet on nonalcoholic fatty liver disease (NAFLD/MAFLD). *J. Clin. Med.* **13**, 4857 (2024).
6. Karin, M. & Kim, J. Y. MASH as an emerging cause of hepatocellular carcinoma: Current knowledge and future perspectives. *Mol. Oncol.* https://doi.org/10.1002/1878-0261.13685 (2024).
7. Pei, K. et al. An overview of lipid metabolism and nonalcoholic fatty liver disease. *Biomed. Res. Int.* **2020**, 4020249 (2020).
8. Yagai, T. & Nakamura, T. Mechanistic insights into the peroxisome proliferator-activated receptor alpha as a transcriptional suppressor. *Front. Med.* **9**, 1060244 (2022).
9. Ebrahimi, R. et al. Adipose tissue gene expression of long non-coding RNAs; MALAT1, TUG1 in obesity: Is it associated with metabolic profile and lipid homeostasis-related genes expression?. *Diabetol. Metab. Syndr.* **12**, 36 (2020).
10. Grabacka, M., Pierzchalska, M., Plonka, P. M. & Pierzchalski, P. The role of PPAR alpha in the modulation of innate immunity. *Int. J. Mol. Sci.* **22**, 10545 (2021).
11. Ortiz, M. et al. Suppression of high-fat diet-induced obesity-associated liver mitochondrial dysfunction by docosahexaenoic acid and hydroxytyrosol co-administration. *Dig. Liver Dis.* **52**, 895–904 (2020).
12. Levine, D. C. et al. NADH inhibition of SIRT1 links energy state to transcription during time-restricted feeding. *Nat. Metab.* **3**, 1621–1632 (2021).
13. Varghese, B. et al. SIRT1 activation promotes energy homeostasis and reprograms liver cancer metabolism. *J. Transl. Med.* **21**, 627 (2023).
14. Liao, J. et al. Formononetin promotes fatty acid beta-oxidation to treat non-alcoholic steatohepatitis through SIRT1/PGC-1alpha/PPARalpha pathway. *Phytomedicine* **124**, 155285 (2024).
15. de Gregorio, E., Colell, A., Morales, A. & Marí, M. Relevance of SIRT1-NF-κB axis as therapeutic target to ameliorate inflammation in liver disease. *Int. J. Mol. Sci.* **21**, 3858 (2020).
16. Meng, D. et al. Biological role and related natural products of SIRT1 in nonalcoholic fatty liver. *Diabetes Metab. Syndr. Obes.* **16**, 4043–4064 (2023).
17. Bianco, A., Tiribelli, C. & Bellarosa, C. Translational approach to the protective effect of bilirubin in diabetic kidney disease. *Biomedicines* **10**, 696 (2022).
18. Jayanti, S., Moretti, R., Tiribelli, C. & Gazzin, S. Bilirubin prevents the TH(+) dopaminergic neuron loss in a parkinson's disease model by acting on TNF-alpha. *Int. J. Mol. Sci.* **23**, 14276 (2022).
19. Shu, X. et al. Association between bilirubin and nonalcoholic fatty liver disease in the non-obese chinese population: A cross-sectional study. *Ann. Transl. Med.* **10**, 522 (2022).
20. Maleki, M. H. et al. Bilirubin improves renal function by reversing the endoplasmic reticulum stress and inflammation in the kidneys of type 2 diabetic rats fed high-fat diet. *Chem. Biol. Interact.* **378**, 110490 (2023).
21. Niknam, M. et al. Bilirubin, an endogenous antioxidant that affects p53 protein and its downstream apoptosis/autophagy-related genes in LS180 and SW480 cell culture models of colorectal cancer. *Biochem. Biophys. Res. Commun.* **672**, 161–167 (2023).
22. Maleki, M. H. et al. Protective and curative effects of unconjugated bilirubin on gene expression of LOX-1 and iNOS in the heart of rats receiving high-fat diet and low dose streptozotocin: A histomorphometric approach. *J. Inflamm.* **21**, 26 (2024).
23. Tavakoli, R. et al. Bilirubin, once a toxin but now an antioxidant alleviating non-alcoholic fatty liver disease in an autophagy-dependent manner in high-fat diet-induced rats: A molecular and histopathological analysis. *Res. Pharm. Sci.* **19**, 475–488 (2024).
24. Liang, C. et al. Association of serum bilirubin with metabolic syndrome and non-alcoholic fatty liver disease: A systematic review and meta-analysis. *Front. Endocrinol.* **13**, 869579 (2022).
25. Bates, E. A. et al. Suppressing hepatic UGT1A1 increases plasma bilirubin, lowers plasma urobilin, reorganizes kinase signaling pathways and lipid species and improves fatty liver disease. *Biomolecules* **13**, 252 (2023).
26. Weaver, L., Hamoud, A. R., Stec, D. E. & Hinds, T. D. Biliverdin reductase and bilirubin in hepatic disease. *Am. J. Physiol. Gastrointest. Liver Physiol.* **314**, G668–G676 (2018).
27. Vitek, L. & Tiribelli, C. Bilirubin: The yellow hormone?. *J. Hepatol.* **75**, 1485–1490 (2021).
28. Vakili, O., Borji, M., Saffari-Chaleshtori, J. & Shafiee, S. M. Ameliorative effects of bilirubin on cell culture model of non-alcoholic fatty liver disease. *Mol. Biol. Rep.* **50**, 4411–4422 (2023).
29. Stocker, R., Yamamoto, Y., McDonagh, A. F., Glazer, A. N. & Ames, B. N. Bilirubin is an antioxidant of possible physiological importance. *Science* **235**, 1043–1046 (1987).
30. Gordon, D. M. et al. Bilirubin remodels murine white adipose tissue by reshaping mitochondrial activity and the coregulator profile of peroxisome proliferator-activated receptor alpha. *J. Biol. Chem.* **295**, 9804–9822 (2020).
31. Gordon, D. M., Hong, S. H., Kipp, Z. A. & Hinds, T. D. Jr. Identification of binding regions of bilirubin in the ligand-binding pocket of the peroxisome proliferator-activated receptor-a (PPARalpha). *Molecules* **26**, 2975 (2021).

32. Creeden, J. F., Gordon, D. M., Stec, D. E. & Hinds, T. D. Jr. Bilirubin as a metabolic hormone: The physiological relevance of low levels. *Am. J. Physiol. Endocrinol. Metab.* **320**, E191–E207 (2021).
33. Zanussi, J. T. et al. Identifying potential therapeutic applications and diagnostic harms of increased bilirubin concentrations: A clinical and genetic approach. *Clin. Pharmacol. Ther.* **111**, 435–443 (2022).
34. Zou, Y. et al. High-fat emulsion-induced rat model of nonalcoholic steatohepatitis. *Life Sci.* **79**, 1100–1107 (2006).
35. Gheibi, S., Kashfi, K. & Ghasemi, A. A practical guide for induction of type-2 diabetes in rat: Incorporating a high-fat diet and streptozotocin. *Biomed. Pharmacother.* **95**, 605–613 (2017).
36. Lin, J. P. et al. Association between the UGT1A1*28 allele, bilirubin levels, and coronary heart disease in the framingham heart study. *Circulation* **114**, 1476–1481 (2006).
37. Dong, H. et al. Bilirubin increases insulin sensitivity in leptin-receptor deficient and diet-induced obese mice through suppression of ER stress and chronic inflammation. *Endocrinology* **155**, 818–828 (2014).
38. Joshi, M. D., Iacoban, P. & Scheetz, M. H. Pharmacokinetic and biomarker quantification studies on vancomycin-loaded PEGylated liposomes and its potential to reduce vancomycin-induced kidney injury: A rat study. *Pharmaceutics* **15**, 1582 (2023).
39. Graves, K. J. et al. Trichomonas vaginalis virus among women with trichomoniasis and associations with demographics, clinical outcomes, and metronidazole resistance. *Clin. Infect. Dis.* **69**, 2170–2176 (2019).
40. Maleki, M. H. et al. Attenuation of brown adipocyte whitening in high-fat diet-induced obese rats: Effects of melatonin and beta-hydroxybutyrate on Cidea, Fsp27 and MT1 expression. *Diabetes Obes. Metab.* **26**, 4551–4561 (2024).
41. Amin, M. A., Ragab, H. M., Abd El Maksoud, N. & Elaziz, W. A. CD24 gene expression as a risk factor for non-alcoholic fatty liver disease. *Diagnostics* **13**, 984 (2023).
42. Weibel, E. R., Kistler, G. S. & Scherle, W. F. Practical stereological methods for morphometric cytology. *J. Cell Biol.* **30**, 23–38 (1966).
43. Rafati, A. et al. Mitigating effect of resveratrol on the structural changes of mice liver and kidney induced by cadmium; a stereological study. *Prev. Nutr. Food Sci.* **20**, 266–275 (2015).
44. Bordbar, H., Soleymani, F., Nadimi, E., Yahyavi, S. S. & Fazelian-Dehkordi, K. A quantitative study on the protective effects of resveratrol against bisphenol a-induced hepatotoxicity in rats: A stereological study. *Iran. J. Med. Sci.* **46**, 218–227 (2021).
45. Karbalay-Doust, S. & Noorafshan, A. Stereological study of the effects of nandrolone decanoate on the mouse liver. *Micron* **40**, 471–475 (2009).
46. von Bartheld, C. S. Distribution of particles in the z-axis of tissue sections: Relevance for counting methods. *Neuroquantology* **10**, 66–75 (2012).
47. Namavar, M. R., Ghalavandi, M. & Bahmanpour, S. The effect of glutathione and buserelin on the stereological parameters of the hypothalamus in the cyclophosphamide-treated mice. *J. Chem. Neuroanat.* **110**, 101871 (2020).
48. Lee, K. et al. A scoring system for the diagnosis of non-alcoholic steatohepatitis from liver biopsy. *J. Pathol. Transl. Med.* **54**, 228–236 (2020).
49. Cioffi, F. et al. Altered mitochondrial quality control in rats with metabolic dysfunction-associated fatty liver disease (MAFLD) induced by high-fat feeding. *Genes* **13**, 315 (2022).
50. Koushki, M. et al. Resveratrol reduces lipid accumulation through upregulating the expression of microRNAs regulating fatty acid bet oxidation in liver cells: Evidence from in-vivo and in-vitro studies. *Iran. J. Pharm. Res.* **19**, 333–340 (2020).
51. Lin, Y., Wang, Y. & Li, P. F. PPARalpha: An emerging target of metabolic syndrome, neurodegenerative and cardiovascular diseases. *Front. Endocrinol.* **13**, 1074911 (2022).
52. Souza-Tavares, H. et al. Peroxisome proliferator-activated receptors as targets to treat metabolic diseases: Focus on the adipose tissue, liver, and pancreas. *World J. Gastroenterol.* **29**, 4136–4155 (2023).
53. Montagner, A. et al. Liver PPARalpha is crucial for whole-body fatty acid homeostasis and is protective against NAFLD. *Gut* **65**, 1202–1214 (2016).
54. Regnier, M. et al. Hepatocyte-specific deletion of Pparalpha promotes NAFLD in the context of obesity. *Sci. Rep.* **10**, 6489 (2020).
55. Purushotham, A. et al. Hepatocyte-specific deletion of SIRT1 alters fatty acid metabolism and results in hepatic steatosis and inflammation. *Cell Metab.* **9**, 327–338 (2009).
56. Liu, X. et al. Silibinin-induced autophagy mediated by PPARalpha-sirt1-AMPK pathway participated in the regulation of type I collagen-enhanced migration in murine 3T3-L1 preadipocytes. *Mol. Cell. Biochem.* **450**, 1–23 (2019).
57. Suh, J. H., Kim, K. H., Conner, M. E., Moore, D. D. & Preidis, G. A. Hepatic PPARalpha is destabilized by SIRT1 deacetylase in undernourished male mice. *Front. Nutr.* **9**, 831879 (2022).
58. Hayashida, S. et al. Fasting promotes the expression of SIRT1, an NAD+ -dependent protein deacetylase, via activation of PPARalpha in mice. *Mol. Cell. Biochem.* **339**, 285–292 (2010).
59. Tutunchi, H. et al. Effects of oleoylethanolamide supplementation on the expression of lipid metabolism-related genes and serum NRG4 levels in patients with non-alcoholic fatty liver disease: A randomized controlled trial. *Clin. Nutr. ESPEN* **58**, 311–319 (2023).
60. Stec, D. E. et al. Bilirubin binding to PPARalpha inhibits lipid accumulation. *PLoS One* **11**, e0153427 (2016).
61. Han, H. et al. Non-linear associations of circulating total bilirubin concentration with the risk of nonalcoholic fatty liver disease and all-cause mortality. *Ann. Hepatol.* **29**, 101177 (2024).
62. Todisco, S. et al. PPAR alpha as a metabolic modulator of the liver: Role in the pathogenesis of nonalcoholic steatohepatitis (NASH). *Biology* **11**, 792 (2022).
63. Yang, Y. et al. Regulation of SIRT1 and its roles in inflammation. *Front. Immunol.* **13**, 831168 (2022).
64. Kauppinen, A., Suuronen, T., Ojala, J., Kaarniranta, K. & Salminen, A. Antagonistic crosstalk between NF-kappaB and SIRT1 in the regulation of inflammation and metabolic disorders. *Cell. Signal.* **25**, 1939–1948 (2013).
65. Zhang, H. N. et al. Involvement of the p65/RelA subunit of NF-kappaB in TNF-alpha-induced SIRT1 expression in vascular smooth muscle cells. *Biochem. Biophys. Res. Commun.* **397**, 569–575 (2010).
66. Katto, J., Engel, N., Abbas, W., Herbein, G. & Mahlknecht, U. Transcription factor NFkappaB regulates the expression of the histone deacetylase SIRT1. *Clin. Epigenet.* **5**, 11 (2013).
67. Lucarelli, R. et al. Eicosanoid-activated PPARalpha inhibits NFkappaB-dependent bacterial clearance during post-influenza superinfection. *Front. Cell. Infect. Microbiol.* **12**, 881462 (2022).
68. Guo, Y. et al. Targeting Sirt1 in a rat model of high-fat diet-induced non-alcoholic fatty liver disease: Comparison of Gegen Qinlian decoction and resveratrol. *Exp. Ther. Med.* **14**, 4279–4287 (2017).
69. Schepis, F., Turco, L., Bianchini, M. & Villa, E. Prevention and management of bleeding risk related to invasive procedures in cirrhosis. *Semin. Liver Dis.* **38**, 215–229 (2018).
70. McConnell, M. J., Kostallari, E., Ibrahim, S. H. & Iwakiri, Y. The evolving role of liver sinusoidal endothelial cells in liver health and disease. *Hepatology* **78**, 649–669 (2023).
71. Altunkaynak, B. Z. & Ozbek, E. Overweight and structural alterations of the liver in female rats fed a high-fat diet: A stereological and histological study. *Turk. J. Gastroenterol.* **20**, 93–103 (2009).
72. Xu, Z. J., Fan, J. G., Ding, X. D., Qiao, L. & Wang, G. L. Characterization of high-fat, diet-induced, non-alcoholic steatohepatitis with fibrosis in rats. *Dig. Dis. Sci.* **55**, 931–940 (2010).
73. Preguica, I. et al. Diet-induced rodent models of obesity-related metabolic disorders-A guide to a translational perspective. *Obes. Rev.* **21**, e13081 (2020).

74. Schroeder, S. M., Matsukuma, K. E. & Medici, V. Wilson disease and the differential diagnosis of its hepatic manifestations: A narrative review of clinical, laboratory, and liver histological features. *Ann. Transl. Med.* **9**, 1394 (2021).
75. Akbari, R. et al. Saroglitazar improved hepatic steatosis and fibrosis by modulating inflammatory cytokines and adiponectin in an animal model of non-alcoholic steatohepatitis. *BMC Pharmacol. Toxicol.* **22**, 53 (2021).
76. Wang, Y. et al. HIIT ameliorates inflammation and lipid metabolism by regulating macrophage polarization and mitochondrial dynamics in the liver of type 2 diabetes mellitus mice. *Metabolites* **13**, 14 (2022).
77. Hinds, T. D. Jr. et al. Mice with hyperbilirubinemia due to Gilbert's syndrome polymorphism are resistant to hepatic steatosis by decreased serine 73 phosphorylation of PPARalpha. *Am. J. Physiol. Endocrinol. Metab.* **312**, E244–E252 (2017).
78. Hinds, T. D. Jr. et al. Bilirubin nanoparticles reduce diet-induced hepatic steatosis, improve fat utilization, and increase plasma beta-hydroxybutyrate. *Front. Pharmacol.* **11**, 594574 (2020).

Acknowledgements

This study is extracted from the master thesis of Motahareh Taghizadeh and was supported by "Grant Number of 25345" from the Vice-chancellor for Research Affairs of Shiraz University of Medical Sciences, Shiraz, Iran.

Author contributions

All authors contributed to the study conception and design. Material preparation, data collection, and analyses were performed by [MT], [MHM], [OV], and [RT]. Bioinformatics investigations, including KEGG and GO analyses, were performed by [PZ]. Histopathological evaluations were carried out by [ARD]. [HB] was responsible for stereological assessments. The first draft of the manuscript was written by [MT], and then edited and improved by [OV]. Supervision and project administration were conducted by [SMS]. All authors read and approved the final manuscript.

Funding

This research was supported by the Vice-chancellor for Research Affairs of Shiraz University of Medical Sciences (Grant No.: 25345).

Declarations

Competing interests

The authors declare no competing interests.

Ethics approval

The study was approved by the Institutional Animal Ethics Committee of Shiraz University of Medical Sciences, Shiraz, Iran (IR.SUMS.AEC.1401.066). Furthermore, the whole study has been reported in accordance with the ARRIVE guidelines 2.0 (ARRIVE Essential 10) https://arriveguidelines.org.

Additional information

Supplementary Information The online version contains supplementary material available at https://doi.org/10.1038/s41598-024-80119-5.

Correspondence and requests for materials should be addressed to S.M.S.

Reprints and permissions information is available at www.nature.com/reprints.

Publisher's note Springer Nature remains neutral with regard to jurisdictional claims in published maps and institutional affiliations.